



# Vegetation index suites as indicators of vegetation state in grassland and savanna: An analysis with simulated SENTINEL 2 data for a North American transect

Michael J. Hill \*

Earth System Science and Policy, University of North Dakota, Grand Forks, ND 58201, USA



## ARTICLE INFO

## Article history:

Received 12 February 2013

Received in revised form 5 June 2013

Accepted 9 June 2013

Available online xxxx

## Keywords:

Vegetation index

Savanna

Grassland

Mixed prairie

Tall grass prairie

Post oak

Sentinel 2

Landsat

Hyperion

## ABSTRACT

Grasslands and savannas form a heterogeneous and patchy mosaic of spectral properties that are challenging for characterization of vegetation states. This study examines the potential for use of suites of vegetation indices (VIs) from the proposed Sentinel 2 sensor to describe vegetation states in grasslands and savannas for a North American transect. Hyperion hyperspectral data from the EO-1 satellite were used to simulate Sentinel 2, MODIS (Moderate Resolution Imaging Spectroradiometer) and VIIRS (Visible Infrared Imaging Radiometer Suite) images for field sites in Alberta, North Dakota and Texas that represent the continuum from short grass prairie to oak savanna and are intermingled with agriculture. Indices representing photosynthetic pigments (Normalized Difference Vegetation Index, Carotenoid Reflectance Index, Anthocyanin Reflectance Index and Red-Green Ratio), vegetation and landscape water content (Normalized Difference Infrared Index), senescent vegetation and soil (Short Wave Infrared Ratio and Plant Senescence Reflectance Index) and herbaceous biomass (Soil Adjusted Total Vegetation Index) were used. There were distinct differences among sites in the relative sensitivity of different VIs depending upon moisture status, tree cover and type of grassland. Simple multi-variate models based on mean values of VIs showed limited ability to predict land cover classes and nominal vegetation states. However, analysis of sample areas using pixels as individual observations within a statistical distribution indicated that subtle variation and gradients within management or land units could be used to characterize fine differences in selected nominal states at each site. Despite some differences in band locations, all VIs except the anthocyanin reflectance index were scalable between Sentinel 2 and MODIS and VIIRS data. A framework for using suites of VIs as indicators of vegetation states that could be applied to the state and transition model approach applied by the US Natural Resource Conservation Service is described. Land types can be effectively characterized by pixel value distribution histograms, and statistical metrics may be used as indicators of status and change. However, time series are needed to fully capture states and state changes, since grasslands and savannas have such high levels of spectral and phenological variation.

© 2013 Elsevier Inc. All rights reserved.

## 1. Introduction

Grasslands and savannas represent a huge area of the terrestrial land surface, and support most of current and future potential land-based food production (Hill & Hanan, 2011). Large scale transitions in vegetation states within these systems may have powerful feedbacks to the Earth system through changes in carbon storage, water and energy balances and atmospheric forcing by fires and aerosols. The definition of vegetation states in grasslands and savannas seems to lend itself to remote sensing applications (Hill, Renzullo, Guerschman, Marks, & Barrett, 2013), however little attention has so far been paid to this potential (Hill, Roman, & Schaaf, 2012). In North America, the grasslands

of the Great Plains stretch from the Rocky Mountains to the eastern deciduous forests and from central Alberta and Saskatchewan to Texas (Conner, Seidl, VanTassel, & Wilkins, 2001). The transition zone between the grasslands and the eastern deciduous forests is represented by an ecotone of oak savannas which originally extended from Texas into Wisconsin and Minnesota (Anderson, 1983; Kuchler, 1975; Leach & Givnish, 1999; McPherson, 1997), but has been heavily converted and fragmented by agriculture.

There is a long history of attempts to utilize remote sensing to objectively characterize the health of xeric herbaceous and tree-grass systems (e.g., Asner & Heidebrecht, 2002, 2003; Asner & Lobell, 2000; Bastin, Ludwig, Eager, Chewings, & Liedloff, 2002; Ludwig et al., 2000; Pickup & Chewings, 1994). In many of these systems, change involves marked changes in soil and vegetation that are not quickly reversible and hence *ad hoc* imagery can be effectively used. The dynamics of semi-arid and more mesic grasslands and savannas requires more frequent observations, more sensitivity to continuous changes, and

\* Tel.: +1 7017776071; fax: +1 7017772940.

E-mail address: [hillmj@aero.und.edu](mailto:hillmj@aero.und.edu).

methods to deal with spectral mixtures. The nature of states detectable with remote sensing depends upon corresponding spectral differences, at a sufficient spatial resolution, and over a time frame that matches multiple imaging frequencies. Thus far, satellite remote sensing has proved more effective at retrieving broad temporal and regional trends in extensive grassland and savanna systems (e.g., the many phenology and productivity assessments; Anyamba & Tucker, 2005; Hill, Vickery, Furnival, & Donald, 1999; Tucker, Justice, & Prince, 1986; Yang, Wylie, Tieszen, & Reed, 1998), than in intensive local monitoring of grassland or savanna condition. Significant progress has recently been made in synthesizing time series of Landsat imagery over savannas, for example (Schmidt, Udelhoven, Gill, & Röder, 2012), using reflectance fusion models such as STARFM (Spatial and temporal Adaptive Reflectance Fusion Model; Hilker et al., 2009). However, these approaches rely on having coverage with the higher resolution data that effectively spans the periods of stable and changing signals so that the time series infill is representative,

The Sentinel 2 sensor system proposed by the European Space Agency will provide a significant improvement in spectral coverage, spatial resolution and temporal frequency over the current generation of Landsat-type sensors (Drusch et al., 2012). The Sentinel 2 mission will have two identical multi-spectral sensors in orbit at the same time delivering a global revisit time of five days. The sensors will have 13 spectral bands at with increased coverage in the red edge, and matching coverage of the short wave infrared to Landsat 8 (Irons, Dwyer, & Barsi, 2012). Full spectral coverage will be available for 20 m spatial resolution (with lesser band coverage at 10 and 60 m) and a 290 km field of view. This sensor potentially provides a huge advance in qualitative and quantitative retrievals and mapping of grasslands and savannas, particularly when combined with Landsat 8 to increase frequency of coverage and with the MODIS (MODerate resolution Imaging Spectroradiometer) and VIIRS (Visible Infrared Imager Radiometer Suite) global imaging systems through further application of reflectance fusion modeling (e.g., Hilker et al., 2009). The potential of hypertemporal analysis with Landsat-class sensors is being already realized through retrospective analysis of very large numbers of images from the Landsat archive (e.g., Potapov et al., 2012).

A number of well-established vegetation indices may be calculated from the Sentinel 2 multispectral bands. Only limited attention has been paid to the potential for suites of vegetation indices to act as indicators of vegetation condition in savannas and grasslands (Hill et al., 2012, 2013). There is a rich history of land systems approaches to remote sensing of rangelands exemplified in the review by Tueller (1989) and the grazing gradient work in Australia (e.g., Pickup & Chewings, 1994). This approach was taken to its natural maturity in arid lands by Asner and Heidebrecht (2002, 2003) using hyperspectral data but there is an opportunity to partially translate the hyperspectral sensitivity into the multispectral domain by making better use of spectral vegetation indices and new sensors. Airborne hyperspectral research has identified a number of narrow band vegetation indices that target particular absorption features strongly related to key chemical and biophysical properties of vegetation and soils (e.g., Sims & Gamon, 2002; Summers, Lewis, Ostendorf, & Chittleborough, 2011; Ustin, Roberts, Gamon, Asner, & Green, 2004; Ustin et al., 2009). Given the complexity of grassland and savanna landscapes across North America, frequent acquisition of suites of vegetation indices with a mechanistic relationship to functional properties of vegetation and landscapes could provide baseline characterization and change detection (Hill et al., 2013). A suite of indices that are sensitive to variation in pigments, water, non-photosynthetic vegetation and soil, and biomass could be combined to form multivariate indicators of vegetation condition. Time series studies with hyperspectral imagery are becoming more common with the availability of a large Hyperion archive globally (e.g., Somers & Asner, 2012, 2013) enhancing potential for development of multivariate indicator approaches from simulation of multispectral sensors.

In this study, we use Hyperion hyperspectral data from the EO-1 satellite (Pearlman et al., 2003) to simulate Sentinel 2, MODIS and VIIRS spectral reflectance, and calculate vegetation indices for two study sites in Alberta (AB), three sites in eastern North Dakota (ND) and one in Texas (TX) that represent a gradient from semi-arid grassland to oak savanna (Fig. 1). The Hyperion sensor on EO-1 has provided the opportunity to test the application of these vegetation indices in space-based imaging within the limitations of modest signal to noise detectors (Middleton et al., 2013). It has also proven valuable in developing measurement of fractional cover and vegetation water content scalable to MODIS (Ferreira et al., 2011; Guerschman et al., 2009). In addition, the Hyperion sensor with its 225 spectral bands provides the spectral coverage to enable simulation of Sentinel 2 imagery for a wide range of global locations prior to launch. The study aims to examine the sensitivity of a suite of Sentinel 2 vegetation indices along a gradient from xeric grasslands to mesic savannas. The study is focused on development of indicators of vegetation condition for landscape or vegetation management units associated with conservation and/or livestock production and in practical application by land management agencies; these units may contain gradients and variation that must be included in assessment, but differentiating between management units is the prime goal. In addition it aims to explore potential scaling relationships between vegetation indices from Sentinel 2, and equivalent or surrogate indices calculated from MODIS and VIIRS given that there are differences band locations and band widths between sensors. Finally the study aims to outline a practical approach to assessment of vegetation states in grasslands and savannas that would assist and complement existing approaches to monitoring of conservation and grazing lands.

## 2. Remote sensing and state and transition modeling

The USDA NRCS (United States Department of Agriculture Natural Resource Conservation Service) is undertaking a comprehensive national ecosystem assessment process (Herrick, Bestelmeyer, Archer, Tigel, & Brown, 2006; Herrick et al., 2010), and grasslands and savannas are a major focus of this assessment. The systematic approach involves landscape stratification, identification of key ecosystem attributes and a spatially explicit and highly integrated approach to ecological characterization, field site selection, data collection and analysis that includes remote sensing. A similar approach to this has been adopted in Alberta (Adams, Poulin-Klein, Moisey, & McNeil, 2004, 2005), Canada with the development of a comprehensive Grassland Vegetation

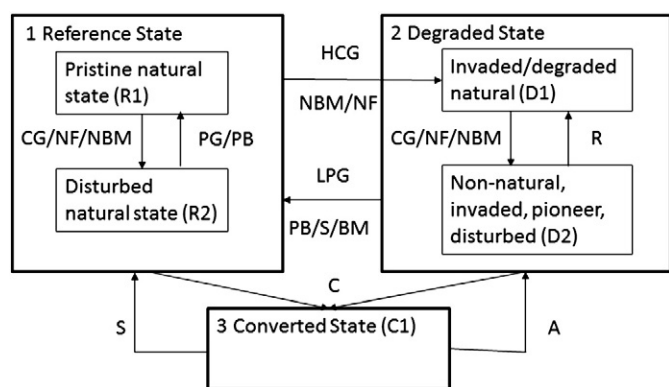


**Fig. 1.** A conceptual S&T framework based on NRCS S&T models for grasslands and savannas in Montana, North Dakota and Texas. The generic states depicted would be targets for discrimination and identification with remote sensing. Transition drivers are as follows: (H)CG—(heavy) continuous grazing; NF—no fire; (N)BM—(no) brush management; (L)PG—(long-term) prescribed burning; PG—prescribed grazing; C—conversion; A—abandonment; S—sowing and planting; and R—resting.

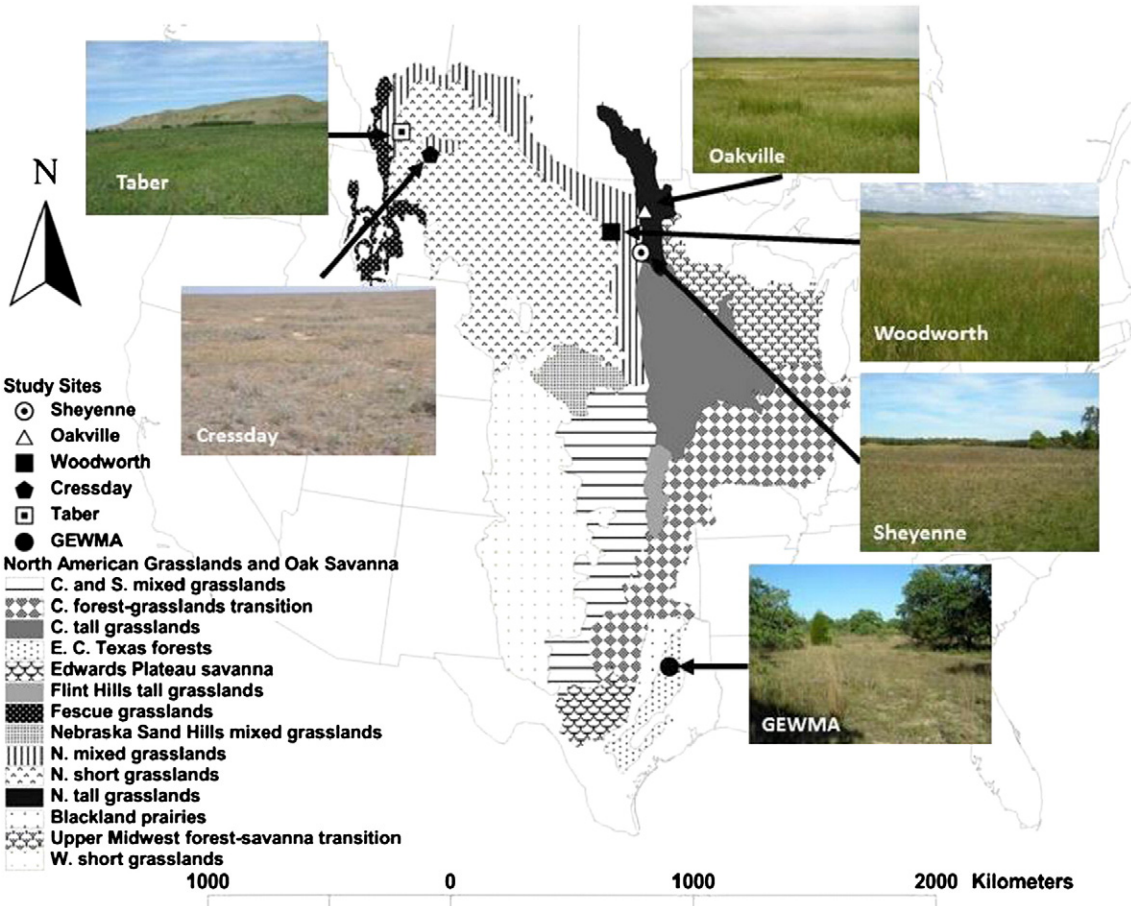
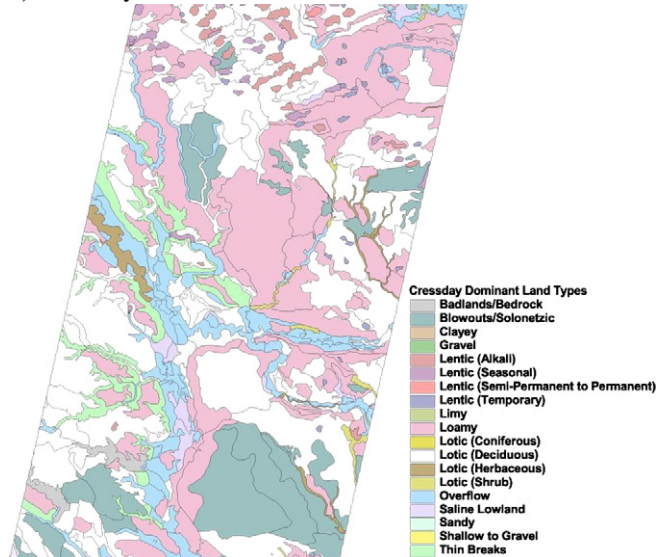


Fig. 2. Map showing the study sites across North America with photos of vegetation cover.

Inventory (GVI; [Government of Alberta, 2010](#)) based on detailed land system characterization and comprehensive site data collection.

In the development of Ecological Site Descriptions (ESDs), detailed S&T models are defined for the vegetation–land system complex ([NRCS, 2011](#)). State and transition models ([Westoby, Walker, & Noy-Meir, 1989](#)) have been widely adopted for detailed understanding and practical management of grazed rangelands ([Bellamy and Brown, 1994; Briske, Fuhlendorf, & Smeins, 2005](#)). Land is characterized

### a) Cressday



### b) Taber

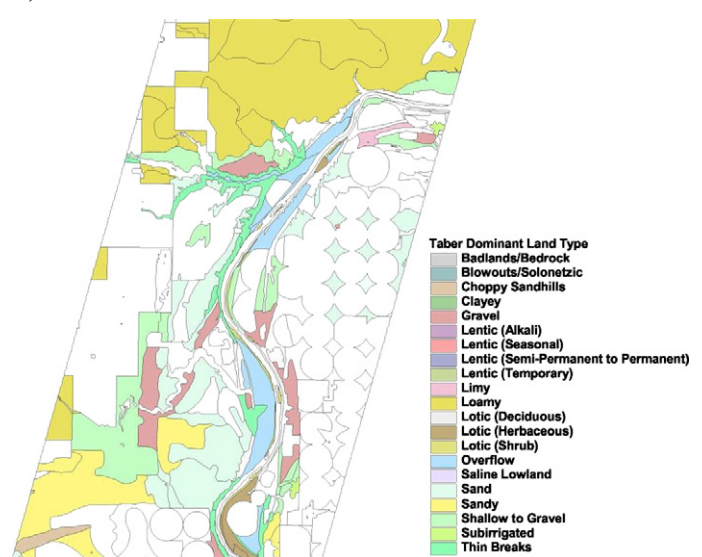
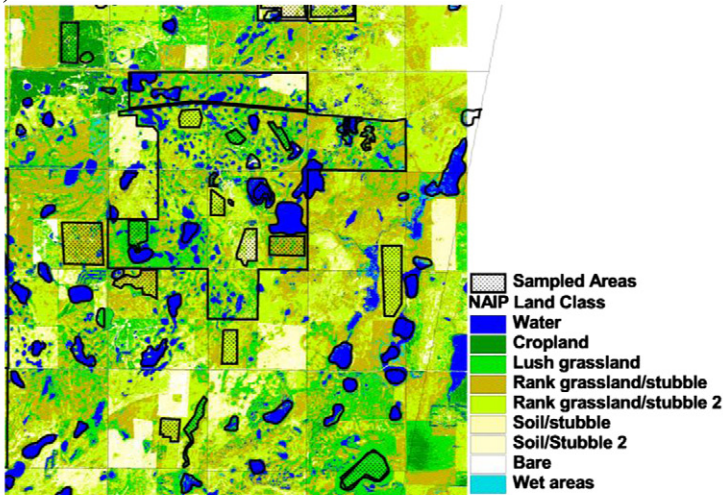
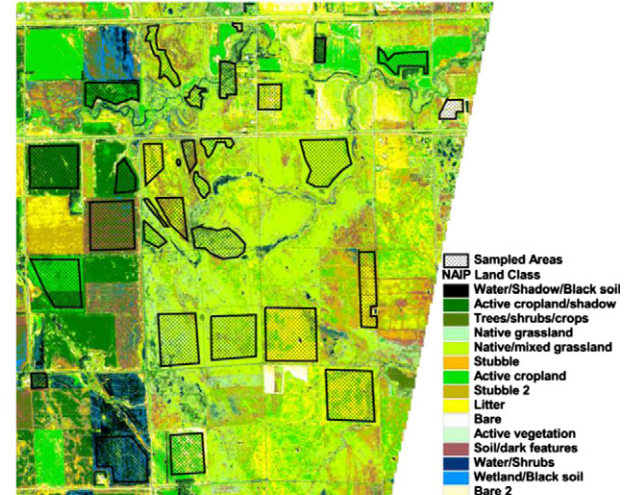


Fig. 3. Study sites in Alberta with full Grassland Vegetation Inventory site type polygon coverage. a) Cressday; and b) Taber. Only polygons with >67% of one GVI site type are colored and sampled. Agricultural areas are excluded for Taber. There is no agriculture at Cressday.

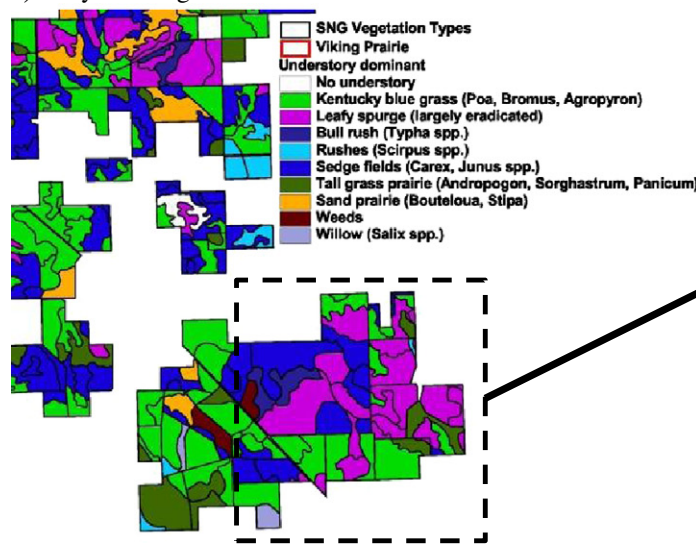
a) Woodworth



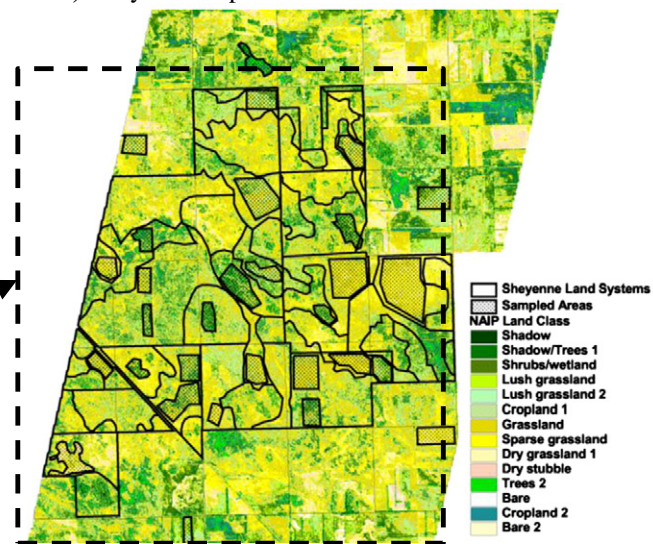
b) Oakville



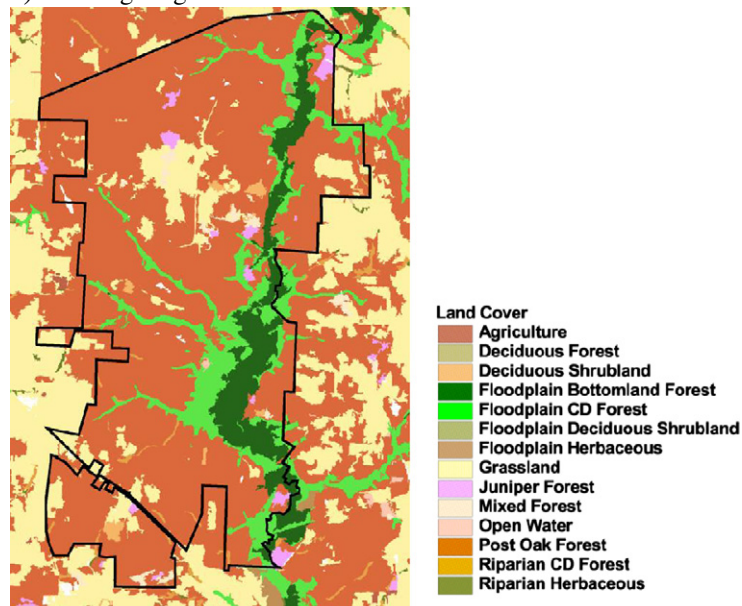
c) Sheyenne vegetation



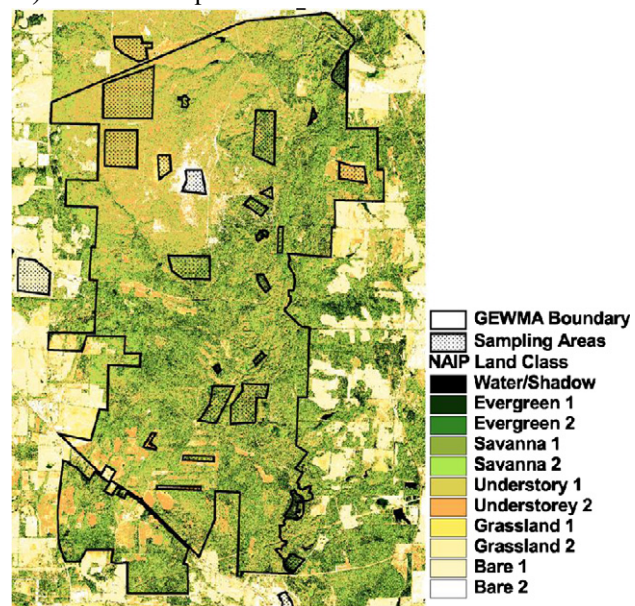
d) Sheyenne airphoto classes



e) Gus Engeling WMA land cover



f) GEWMA air photo classes



by different vegetation states, and transitions between these states, such as perennial to annual grassland, or woody thickening of grassland occur as a result of defined drivers such as fire, grazing and drought. Although not widely applied outside the range community, S&T models have potential to improve understanding, modeling and management across a wide range of ecosystem types (Bestelmeyer, Goolsby, & Archer, 2011; Hill, Roxburgh, Carter, & McKeon, 2005; Jeltsch, Tietjen, Blaum, & Rossmannith, 2011; Weber, Moloney, & Jeltsch, 2000). Nominal states are represented by a combination of land cover and land use. Transitions are assumed to occur as a result of land cover and land use change, combined with land management practices and interaction with weather and invasive species. In rangeland applications these S&T models can be highly complex with states defined by changes in botanical composition linked to both drivers and successional processes (e.g., Ash, Bellamy, & Stockwell, 1994; Filet, 1994; NRCS, 2011, 2012a, b, c).

The NRCS has developed S&T models to correspond to all of the distinct ecological regions they are characterizing (NRCS, 2011, 2012a, b, c). For the purposes here, a generic version of the state and transition model structure is shown in Fig. 1. The fundamental basis for these models lies in the definition of an original, pristine Reference state which represents the original undisturbed vegetation (R1). This may be slightly perturbed to R2 by continuous grazing (CG), lack of fire (NF) and lack of brush management (NBM) but readily returned to R1 by prescribed burning (PB) and prescribed grazing (PG). However heavy continuous grazing (HCG) combined with NBM and NF can result in transition to a Degraded state (D1) with further pressure resulting in further degradation to D2. These degraded systems can only be returned to R1 or R2 through long term PG, PB, BM and seeding with native grasses. These states are often shifted permanently to Converted (C1) for agriculture.

Grasslands and savannas form a heterogeneous and patchy mosaic of spectral properties that are challenging for characterization of vegetation states in terms of meaningful properties (Hill and Hanan, 2011). Some basic guidelines for developing a soil-vegetation monitoring system in rangelands were outlined by Havstad and Herrick (2003): a) identify suites of indicators correlated with critical ecosystem processes or properties; b) establish baseline indicators for site specific purposes and local soil and site characteristics; c) incorporate spatial variability to make indicators more representative; d) interpret indicators within a framework of dynamic and non-linear processes. The key to effective use of medium resolution (20–30 m pixels) optical remote sensing to characterize vegetation states in grasslands and savannas lies in development of spectral indicators that are sensitive to changes in vegetation properties and cover that are linked to ecosystem function. The new high frequency multispectral remote sensing capability promised by Sentinel 2 (and combined with Landsat 8) implies that this domain of sensitivity can be defined by the quantitative metrics retrieved from spatial and temporal properties of a suite of VIs that maximize the spectral sensitivity to functional attributes.

The major difficulty encountered in demonstrating the application of VI suites as state indicators arises from interpreting available land cover and land use information into approximate examples of vegetation states that could reasonably correspond to the conceptual states in Fig. 1. In practice, a monitoring regime for particular areas would have specific state definitions and calibrated indicators of states from VI suites. This analysis represents the first stage prototyping of this approach. Therefore, initially, suites of VIs are examined in relation to available land cover classifications, augmented with local knowledge where possible. Subsequently, the available land cover information is nominally allocated

to conceptual states from Fig. 1, in order to illustrate the potential and the limitations.

### 3. Methods

#### 3.1. Site descriptions

The sites represent a continuum from the xeric mixed prairie (Cressday, AB), through more mesic mixed prairie (Taber, AB), to mixed grass prairie (Woodworth, ND) and saline tall grass prairie (Oakville, ND), to a mixed landscape of tall grass prairie, oak savanna and eastern forest (Sheyenne National Grassland (SNG), ND), and finally into Post oak savanna (Gus Engeling Wildlife Management Area (GEWMA), TX; Fig. 2). This continuum spans the grassland and tree-grass ecotone from west to east and north to south in North America.

##### 3.1.1. Southern Alberta

Southern Alberta contains a gradient of successively more xeric grassland associations with eastward distance from the Rocky Mountains (Fig. 2). Fescue grasslands occur in the foothills of the Rocky Mountains (Foothills fescue; *Festuca campestris*; Adams, Ehlert, Moisey, & McNeil, 2003), and in a band (Plains fescue; *Festuca hallii*) across the plains between the mixed prairie and the Aspen Parklands (Burkinshaw, Willoughby, France, Loonen, & McNeil, 2009). The plains are made up of the dry mixed prairie (dominated by *Pascopyron dasystachium*, *Stipa comata*; Adams et al., 2005) on the eastern areas (Cressday site; Fig. 3a) dominated by cattle grazing and the mixed grass prairie (dominated by *S. comata*, *Koeleria cristata*, *Pascopyron smithii*; Adams et al., 2004) intermingled with irrigated and dryland agriculture (Taber site; Fig. 3b). Conversion to agriculture is an on-going threat to mesic prairie grasslands in southern Alberta. Mixed prairie rangeland is sensitive to overgrazing and drought which can result in major wind erosion on land susceptible to "blowouts" (see land classes, Fig. 3). Leafy spurge (*Euphorbia esula*) is a major invasive species in more mesic rangeland (Adams et al., 2004).

##### 3.1.2. North Dakota

Eastern ND is heavily converted to agriculture but contains remnants of tall grass prairie and increasing presence of sown grasslands and Conservation Reserve Program (CRP) land westward into the Prairie Pothole Region (PPR). In the PPR, there are major areas of CRP and federal and state conservation land, often sown down to exotic smooth bromegrass (*Bromus inermis*) surrounding permanent wetlands (Woodworth site; Fig. 4a). Major tall grass prairie remnants are confined to non-arable soil types, and includes remnant saline prairie in Grand Forks County (Oakville site; Fig. 4b), and the SNG (Fig. 4c, d). Within the saline tall grass prairie lands in Grand Forks County, the Oakville prairie is pristine and dominated by Canada wildrye (*Elymus canadensis*), wheat grasses (*Pascopyron* spp.), June grass (*Koeleria macrantha*) and prairie cord grass (*Spartina pectinata*; Facey, La Duke, & Wyckoff, 1986). The site is mostly too wet to support other tall grasses. Surrounding grasslands are largely heavily altered and invaded with smooth bromegrass (*B. inermis*) (Fig. 4b).

The SNG contains a diversity of landscapes which support eastern forest, oak savanna (*Quercus* spp.), cottonwood (*Populus deltoides*) groves on old dust bowl blowouts, sand hills, hummock and swale and deltaic lands, and significant areas of the invasive Kentucky blue grass (*Poa pratensis*) and leafy spurge (*E. esula*; Svingen, Braun, & Gonzalez, 2008; Fig. 4c). The Viking Prairie on the northern border of

**Fig. 4.** Study sites in ND and Texas having high resolution aerial photography. Images (a, b, d, f) show classified aerial photographs overlaid with the polygons used to sample vegetation types based on land cover classes and air photo classes. Land cover classification maps are also shown where available (c, e). a) Woodworth classified aerial photo; b) Oakville classified aerial photo; c) Sheyenne understory land cover; d) Sheyenne classified aerial photo; and e) GEWMA land cover classification; and f) GEWMA classified aerial photo. In a), the large central polygon shows the outline of the Chase Lake National Wildlife Refuge.

the Sheyenne (not shown in Figure) is a single quarter section containing essentially pristine tall grass prairie made up of little bluestem (*Schizachyrium scoparium*), big bluestem (*Andropogon gerardii*), Indian grass (*Sorghastrum nutans*), switchgrass (*Panicum virgatum*), northern reed grass (*Calamagrostis stricta* ssp. *inexpansa*), prairie cord grass (*S. pectinata*) and associated short grasses, forbs and herbs.

### 3.1.3. Texas

Originally, a contiguous grassland–forest transition zone of oak savanna ran through the eastern edge of the US Great Plains. This has been heavily converted and fragmented, but many remnants remain characterized by a variety of oak trees and understory warm season grasses (Fig. 1). At GEWMA site in TX (Fig. 4e, f), historical grazing has degraded understory little bluestem (*S. scoparium*) grassland, and fire suppression has encouraged thickening of Post oak (*Quercus stellata*) savanna and invasion by evergreens such as eastern red cedar (*Juniperus virginiana*) and yaupon (*Ilex vomitoria*) (Cathey, Mitchell, Prochaska, DuPree, & Sosebee, 2006). The Texas Parks and Wildlife Department continues to undertake savanna restoration which involves clearing, thinning, burning and re-establishment of grassland.

### 3.2. Image processing

EO-1 Hyperion images were acquired over all but one of the study sites in 2009: Cressday, AB, August 17; Taber, AB, August 1; Oakville Prairie, ND, September 1; Woodworth, ND, September 22; GEWMA, TX, August 24. An image over SNG, ND was acquired from the online archive to complete the site coverage, July 7, 2011. Late summer images were selected to provide a mixture of green and senescent vegetation cover. The images were radiometrically calibrated and atmospherically corrected using ACORN 6.1<sup>R</sup>. The imagery was processed to remove bad bands, de-striping, remove noise from the short wave infrared region, and remove the major water interference regions following a comprehensive suite of procedures (Apan, Held, Phinn, & Markley, 2004; Datt, McVicar, Van Niel, Jupp, & Pearlman, 2003; Datt & Jupp, 2004; Jupp, Datt, Lovell, Campbell, & King, 2002). The final images contain 152 bands for subsequent analysis—this retained the following wavelength ranges: 447–1114 nm; 1154 nm–1336 nm; 1487–1790 nm; and 1981–2365 nm. Images were geometrically corrected using image to image registration from geometrically corrected Landsat data with a first degree polynomial transform. The RMSE (Root Mean Square Errors) ranged from 0.3 to 0.4 pixels. Images were subjected to small shifts in post processing to ensure the best alignment with the vector polygon data for roads and land management units.

Hyperspectral images were then spectrally resampled in the ENVI® image processing system to Sentinel 2, MODIS, and VIIRS bands using lookup tables for band centers and the full width half maximum (FWHM) of the band pass (Table 1). The signal to noise ratios (SNR) for the proposed Sentinel 2 bands range from 168 for 560 nm to 100 for 2190 nm; SNR is 174 for the broad band at 845 nm, and 72 for the narrow band at 865 nm (Drusch, Gascon, & Berger, 2010). Hyperion provides reasonably comparable SNR in the visible and near infrared (161 at 550 nm, 147 at 700 nm and 110 at 1125 nm) but significantly lower SNR in the SWIR (40 at 2125 nm). Hence the simulated SWIR channels for Sentinel 2 have lower fidelity than would be available from the actual sensor. These images were then spatially resampled to expected spatial resolutions for Sentinel 2 at 20 m, MODIS at 500 m, and VIIRS at 750 m. Both VIIRS and MODIS have finer spatial resolutions for red and NIR bands and NDVI products (375 and 250 m respectively), but we are concerned here with accessing the broadest possible spectral sensitivity, hence the best available spatial resolutions for full spectral retrieval are used. Linear interpolation was used to resample down from the 30 m pixel resolution of Hyperion to the 20 m pixel resolution of Sentinel 2, and pixel aggregation was used to resample up to MODIS and VIIRS resolution.

**Table 1**

Band locations(λ) and widths(FWHM) for Sentinel 2, MODIS and VIIRS showing approximate correspondence among land (L), ocean (O), atmosphere (A) and cloud (C) bands (Code based on MODIS), and whether simulated with Hyperion.

Sentinel 2 (nm)	FWHM	MODIS		VIIRS		Hyperion
		(nm)	FWHM	(nm)	FWHMF	
443	20	412.50	15	412	20	No
		4420	10	445	18	No
		469 L	20			Yes
490	65	4880	10	488	20	Yes
		5310	10			Yes
		5510	10			Yes
560	35	555 L	20	555	20	Yes
		645 L	50	640	80	Yes
		6670	10	672	20	Yes
		6780	10			Yes
705	15					Yes
		7480	10	746	15	Yes
		20				Yes
783	115	858 L	35			Yes
		869.50	15	865	39	Yes
		936/940A	10/50			Yes
		1240 L	20	1240	20	Yes
1375	30	1375C	30	1378	15	No
		1640 L	24	1610	60	Yes
1610	90			2250	50	Yes
		2130 L	50			Yes
2190	180					

A suite of narrow band vegetation indices sensitive to specific absorption features and spectral responses associated with vegetation properties particularly important in the grassland–savanna domain were selected (Table 2). These indices had to be calculable with Sentinel 2 bands and have corresponding equivalent or surrogate bands for MODIS and VIIRS. Indicator indices were chosen as best representatives of vegetation indices sensitive to four key categories of vegetation/soil properties:

1. Photosynthetic pigments. The NDVI (Normalized Difference Vegetation Index; Tucker, 1979) is representative of a large number of variants sensitive to chlorophyll and photosynthetic vegetation (PV). The CRI1 (Carotenoid Reflectance Index I; Gitelson, Zur, Chivkunova, & Merzlyak, 2002) is sensitive to yellow pigments and all three simulated sensor band locations have reasonable matches. The ARI1 (Anthocyanin Reflectance Index I; Gitelson, Merzlyak, & Chivkunova, 2001) is a narrow band index sensitive to red pigments and hence may be useful in detecting stress or waterlogging. Neither VIIRS nor MODIS had a band at 700 nm, hence for the ARI1, we examine scaling relationships with a pseudo-ARI1 (psARI1) using the nearest available spectral band to 700 nm (see Tables 1 and 2). The RGR (Red Green Ratio; Sims & Gamon, 2002) is a broad band index also sensitive to red pigments but readily calculable from all multispectral sensors. Hence it may be regarded as a (less sensitive) substitute where wavelengths for ARI1 are not available.
2. Vegetation and landscape water content. The NDII (Normalized Difference Infrared Index; Hardisky, Klemas, & Smart, 1983) utilizes the 1610 nm band available from Sentinel 2 and VIIRS, and the 1640 nm available from MODIS, and is a little more robust in dryland environments (e.g., Hill et al., 2013) than the NDWI which uses the 1240 nm band of MODIS (Normalized Difference Water Index; Gao, 1996).
3. Senescent (non-photosynthetic) vegetation and soils. The SWIR32 (Short Wave Infrared Ratio) also uses the bands in the 1610–1640 nm range and has been used as a surrogate for the CAI (Cellulose Absorption Index; Nagler, Inoue, Glenn, Russ, & Daughtry, 2003) in scaling fractional cover estimation from Hyperion to MODIS bands (Guerschman et al., 2009). The response space between NDVI and SWIR32 can be used to estimate fractional cover of PV,

**Table 2**

Hyperspectral narrow band vegetation indices multi-spectral equivalents and surrogates for Sentinel 2, MODIS and VIIRS. For SATVI, L is assumed to be 0.5 in the absence of soil line analysis.

Hyperspectral Broad and Narrow-Band Vegetation Index	Narrow Band Formula	Sentinel 2 Equivalent or Surrogate	MODIS Equivalent or Surrogate	VIIRS Equivalent or Surrogate
NDVI (Normalized Difference Vegetation Index)	$\frac{(R_{803} - R_{681})}{(R_{803} + R_{681})}$	$\frac{(R_{865} - R_{665})}{(R_{865} + R_{665})}$	$\frac{(R_{858} - R_{645})}{(R_{858} + R_{645})}$	$\frac{(R_{865} - R_{640})}{(R_{865} + R_{640})}$
CRII (Carotenoid Reflectance Index I; Gitelson et al., 2002)	$\left(\frac{1}{R_{510}}\right) - \left(\frac{1}{R_{550}}\right)$	$\left(\frac{1}{R_{490}}\right) - \left(\frac{1}{R_{560}}\right)$	$\left(\frac{1}{R_{488}}\right) - \left(\frac{1}{R_{555}}\right)$	$\left(\frac{1}{R_{488}}\right) - \left(\frac{1}{R_{555}}\right)$
ARI1 (Anthocyanin Reflectance Index; Gitelson et al., 2001)	$\left(\frac{1}{R_{550}}\right) - \left(\frac{1}{R_{700}}\right)$	$\left(\frac{1}{R_{560}}\right) - \left(\frac{1}{R_{705}}\right)$	$\left(\frac{1}{R_{555}}\right) - \left(\frac{1}{R_{678}}\right)$	$\left(\frac{1}{R_{555}}\right) - \left(\frac{1}{R_{672}}\right)$
RGR (Red-Green Ratio; Sims & Gamon, 2002)	$\frac{R_{600-690}}{R_{500-590}}$	$\frac{R_{665}}{R_{560}}$	$\frac{R_{645}}{R_{555}}$	$\frac{R_{672}}{R_{555}}$
NDII (Normalized Difference Infrared Index; Hardisky et al., 1983)	$\frac{(R_{819} - R_{1649})}{(R_{819} + R_{1649})}$	$\frac{(R_{842} - R_{1610})}{(R_{842} + R_{1610})}$	$\frac{(R_{858} - R_{1640})}{(R_{858} + R_{1640})}$	$\frac{(R_{865} - R_{1610})}{(R_{865} + R_{1610})}$
PSRI (Plant Senescence Reflectance Index; Merzlyak et al., 1999)	$\frac{(R_{860} - R_{560})}{(R_{750})}$	$\frac{(R_{865} - R_{560})}{(R_{740})}$	$\frac{(R_{645} - R_{531})}{(R_{748})}$	$\frac{(R_{672} - R_{555})}{(R_{746})}$
SATVI (Soil Adjusted Total Vegetation Index; Marsett et al., 2006)(Landsat-based)	$\frac{\left(\frac{(R_{1650} + R_{680})}{(R_{1650} + R_{680} + L)}\right)}{(1 + L) - \frac{R_{2115}}{2}}$	$R_{1610}, R_{665}, R_{2190}$	$R_{1640}, R_{645}, R_{2130}$	$R_{1650}, R_{640}, R_{2250}$
CAI (Cellulose Absorption Index; Nagler et al., 2003); SWIR32 (Short Wave Infrared Reflectance 3/2 Ratio; Guerschman et al., 2009)	$0.5(R_{2000} + R_{2200}) - R_{2100}$	$\frac{R_{2100}}{R_{1610}}$	$\frac{R_{2130}}{R_{1640}}$	$\frac{R_{2250}}{R_{1610}}$

NV and bare soil. The PSRI (Plant Senescence Reflectance Index; Merzlyak, Gitelson, Chivkunova, & Rakitin, 1999) utilizes narrow bands within the VNIR spectral region; however there is significant variation among Sentinel 2, MODIS and VIIRS in band centers for green and red wavelengths.

4. Grassland biomass. Grassland biomass has frequently been correlated with NDVI, categorized under pigment indices above, and other red edge indices, however sensitivity to mixed or predominantly senescent grassland found across rangelands and savannas may be provided by the SATVI (Soil Adjusted Total Vegetation Index; Marsett et al., 2006), developed for the arid grasslands of Arizona and New Mexico.

### 3.3. Detailed examination of land cover classes and nominal vegetation states

The analysis involved two levels of assessment:

1. Suites of vegetation indices were examined in relation to the land cover classes.
2. Suites of vegetation indices were examined in relation to nominal vegetation states based on interpretation of land cover classes to the framework in Fig. 1.

#### 3.3.1. Alberta: GVI site types as land cover classes

At Cressday and Taber (Fig. 3), the Alberta Grassland Vegetation Inventory (GVI; Government of Alberta, 2010) is used to represent the mixed prairie landscape. The GVI is based on a combination of soil and landform data, and digital color infrared stereo photography. It is primarily a biophysical and land use inventory and so does not directly document vegetation beyond the level of cropland, grassland, wetland, shrubs, trees and bare areas. The polygons are indicative of uniformity of biophysical areas such as grassland on different soils and the base unit is defined as the Site Type. The GVI polygons can contain up to three Site Types defined by percentage cover: for example a polygon could be predominantly loam, but contain small areas of badlands and blowouts. The polygon may also have entries documenting the percentage of grassland, non-vegetated area or shrubs. In order to limit variability in signals due to divergent mixtures within polygons, yet retain a large number of separate polygons, only non-agricultural polygons where polygons contained >67% of a single Site Type were used. The mean and standard deviation of the vegetation indices, and the pixel distribution histograms were extracted for each polygon at each site. There were multiple polygons of each GVI Site Type.

#### 3.3.2. Sites in the USA: aerial photo classification combined with land cover/use data

At Oakville, Woodworth, SNG and GEWMA National Agriculture Imagery Program (NAIP) aerial photos (red, green blue intensity bands) were classified using an unsupervised isodata method in the ENVI® image processing software and aggregated to between 9 and 15 classes depending upon the variation in each scene (Fig. 4). In North Dakota, these classified images were overlaid with polygon boundaries for sections, School Trust Lands, and United States Fish and Wildlife Service lands (Fig. 4a, b). At SNG, polygon data defining section boundaries and vegetation types from a comprehensive vegetation survey of the grassland (Svingen et al., 2008) were also overlaid and used to identify contiguous vegetation types (Fig. 4c, d). At GEWMA, merged polygon data for original Texas land allocations (data not shown), the boundary for the wildlife management area, and land cover boundaries from the Texas Parks and Wildlife Department Phase 2 mapping of existing vegetation of Texas (Fig. 4e; East Texas at fine scale; Ludeke, German, & Scott, 2009) were used in conjunction with the classified aerial photo (Fig. 4f).

Based on the overlaid geographic data and local knowledge of the sites (the author is personally familiar with all of them), sets of polygons were digitized (shown as small hatched areas in Fig. 4) within known management boundaries and for areas representative of major vegetation and land types with uniform, or uniformly varied aerial photo class compositions. These polygons were then labeled with a land cover class based on the land use, third party land cover classification and the aerial photo class composition: some were unique and some had multiple polygons. Mean and standard deviation, and pixel distribution histogram for each VI was then extracted using the polygon layers at each site.

#### 3.3.3. Assignment of nominal vegetation states

The sample polygons at each study site were assigned to nominal vegetation state (Table 3) based on heuristics and information from NRCS S&T models, and approximating states in Fig. 1. The R1 state is the most problematic, since so much of the North American landscape has been affected by indirect changes to grazing and fire regimes. However, from personal observation it was reasonable to assign R1/R2 status to grasslands on loamy GVI site types in southern Alberta (Fig. 3a, b), R1 status to the saline grassland at Oakville which has never been ploughed (Fig. 4b), R1 status to a relatively pristine tall grass prairie at Viking near SNG (not shown), and R1 status to flooded bottomland forest at GEWMA (Fig. 4e). Based on photographs, the School Trust Land near Woodworth (Fig. 4a) can be assigned an R2 status since this land is grazed but never ploughed. It was substantially easier to select vegetation cover polygons for the D1/D2 and C1 states; rank grassland

Table 3

Descriptions of vegetation states by site. The states are identified by the code shown in Fig. 10. State plotted as frequency distribution VI indicators in Fig. 10 are identified by the curve color used.

Description	State	Color
<b>Cressday, AB Dry mixed prairie</b>		
Grassland on loams – <i>Stipa comata</i> , <i>Pascopyrum dasystachyum</i>	R1/R2	Green
Grassland on blowout soils – <i>Stipa comata</i> , <i>Koeleria cristata</i>	D1	Yellow
Badlands (natural but a surrogate for severe degradation)	D2	Red
<b>Taber, AB Mesic mixed prairie</b>		
Grassland on loams – <i>Stipa comata</i> ; <i>Pascopyrum dasystachyum</i> , <i>Festuca campestris</i>	R1/R2	Green
Grassland on blowout soils	D1	Yellow
Badlands (natural but a surrogate for severe degradation)	D2	Red
Tame pasture	C1	Red
<b>Woodworth, ND Mixed grass prairie</b>		
School Trust Grassland – mixed forbs, C# grasses with some invasives	R2/D1	Green
Exotic conservation grassland ( <i>Bromus inermis</i> )	D2	Yellow
Agriculture	C1	Red
<b>Oakville, ND Tall grass prairie - saline</b>		
Saline tallgrass prairie – <i>Pascopyrum dasystachyum</i> , <i>Koeleria pyramidata</i> , <i>Elymus canadensis</i> , <i>Spartina pectinata</i> , <i>Carex</i> spp. <i>Aster</i> spp. <i>Helianthus</i> spp.	R1	Green
School Trust grasslands – as above plus <i>B. inermis</i> , thistles, sweet clover etc	R2/D1	Green
Altered grassland – mixed species including <i>Pascopyrum</i> spp., <i>B. inermis</i> , <i>Poa pratense</i> , weeds	D1	Yellow
Heavily grazed grassland	D2	Magenta
Agriculture	C1	Red
<b>Sheyenne, ND Tall grass prairie; oak savanna</b>		
Viking tall grass prairie	R1	Green
<i>Panicum virgatum</i> /Carex spp grasslands	R2	Green
<i>Panicum virgatum</i> / <i>Poa pratense</i> grassland	D1	Yellow
<i>Euphorbia esula</i> / <i>Poa pratense</i> grassland	D2	Magenta
Agriculture	C1	Red
<b>Gus Engeling WMA, TX Oak savanna</b>		
Flood bottomland forest	R1	Green
<i>Quercus stellata</i> woodland – thickened	R2	Green
<i>Quercus stellata</i> / <i>Juniperus virginiana</i> – invaded woodland	D1	Magenta
<i>Schizachyrium scoparium</i> degraded grassland	D1	Yellow
<i>Juniperus virginiana</i>	D2	Magenta
Tame pastures	C1FWHM	Red

at Woodworth and mixed grassland at Oakville (Fig. 4a, b), Kentucky blue grass (Fig. 4c) on lush grassland (Fig. 4d) at SNG, and Juniper forest (Fig. 4e) and Evergreen 1 and 2 (Fig. 4f) at GEWMA all reasonably represent D1/D2 states; and agriculture at ND sites and tame pasture around GEWMA represents C1. For the Alberta sites, in the absence of more detail on vegetation cover, only the most extreme GVI site types were selected to represent the most degraded vegetation (D1/D2) states (blowout soils and badland areas) that were most likely to provide extreme conditions that might correspond most closely to those states.

### 3.3.4. Statistical analysis

Two contrasting analytical approaches were applied. In the first, it was assumed that the mean value of a VI was representative of any

target polygon describing vegetation class or vegetation state. As a further refinement, the land cover classes (Fig. 4) were nominally allocated to vegetation states approximating the main states in Fig. 1. For this analytical approach, nominal vegetation states were not allocated for the Alberta sites, since there were many GVI Site Types that support grassland and preliminary assessment indicated that within-class variation in VI signals was as large as between-class variation.

A simple multivariate modeling approach was applied using the vegetation indices as continuous variables to predict land cover classes and nominal vegetation states. The predicted land cover classes and vegetation states were then compared with the expected classes and states in a contingency table analysis. This analysis is described by: the  $R^2_u$  (the ratio of the negative log-likelihood of the predicted

response divided by the negative log-likelihood of the expected response), a measure of the uncertainty explained by the model fit; the Likelihood Ratio Chi-squared test (based on the difference in log-likelihoods between the whole population and the individual responses), a measure of the similarity of response between predicted and expected; and the Kappa statistic (Agresti, 1990), a measure of the agreement between the predicted and expected classes.

In the second approach, the vegetation condition of each sample polygon was regarded a more complex function of the value distribution of the VI pixels in each area. In this case, for demonstration purposes, a very limited subset of GVI Site Types was selected to reasonably correspond to the major conceptual vegetation states. In this case only extreme GVI site types were used to avoid confounding affects. Thus, each polygon representing land condition or vegetation state would have a set of eight pixel value distribution curves with all of the attendant attributes of a statistical distribution including the mean, median, standard deviation, and measures of shape such as skewness and kurtosis. If an assumption of normality is applied, then these distributions can be compared using the Z statistic.

$$Z = \frac{(X_1 - X_2)}{\sqrt{(\sigma_{X_1}^2 + \sigma_{X_2}^2)}}$$

where  $X_1$  and  $X_2$  are the means, and  $\sigma_{X_1}$  and  $\sigma_{X_2}$  are the standard deviations of the pixel distributions for polygons 1 and 2 divided by the square root of the number of pixels for each polygon. This test can probably be safely used as long as distributions are reasonably close to normal. Highly skewed pixel distributions would invalidate this test, but other statistics such as the median, skewness and kurtosis as well as heuristic shape comparison could then be used. Here this test has been used for all distributions for demonstration purposes.

#### 3.4. Scaling analysis

At each study site, the image data were clipped to a region surrounding the field site. Simulated MODIS and VIIRS VI data were scaled (multiplied by 1000), integerized, and converted to polygons

representing MODIS and VIIRS grid cells having the same VI values. These layers were then used to extract the mean and standard deviation from the Sentinel 2 index layers corresponding to each VI value at MODIS and VIIRS scale. Mean and standard deviation data were plotted against MODIS and VIIRS VI values, and linear regressions were fitted to relationships between VIIRS and MODIS values and mean Sentinel 2 values at each site for each VI.

## 4. Results

### 4.1. Variation across study sites

The sites showed some variation in the pattern of correlation among vegetation indices (Fig. 5). Correlations between indices from simulated Sentinel 2 data were relatively weaker at Cressday and Woodworth and relatively stronger at Oakville, Sheyenne and GEWMA. NDVI, CRI1 and ARI1 were strongly positively correlated. They tended to be strongly negatively correlated with RGR, PSRI and SWIR32. SATVI was less well correlated with the other indices and correlations varied between sites.

The spatial variation in relation to reference land cover boundaries is illustrated for the dry mixed prairie site, Cressday (Fig. 6a), and the post oak savanna site, GEWMA (Fig. 6b) with a subset of indices. At Cressday indices show broadly similar patterns in relation to water courses and the presence of thick herbaceous or woody vegetation, and alkali or badland areas with little vegetation (Fig. 6a). The dynamic range of all indices is small at this dry site, but subtle variations in pattern are evident between different indices on extensive upland grassland areas. At GEWMA, the outline of the wildlife management area (WMA) is clearly seen in NDVI and CRI1 in particular (Fig. 6b). With the full range of cover from riparian vegetation and bottomland forest through savanna to bare areas (see Fig. 4e), the dynamic range of all indices is large. High values of SWIR32 and SATVA are found in the open grassland and bare areas corresponding respectively to sensitivity to both soil and senescent vegetation, and herbaceous biomass. Lower NDVI and NDII and higher SWIR32 areas in the west central area correspond to the main area of sandy soil and thickened post oak savanna.

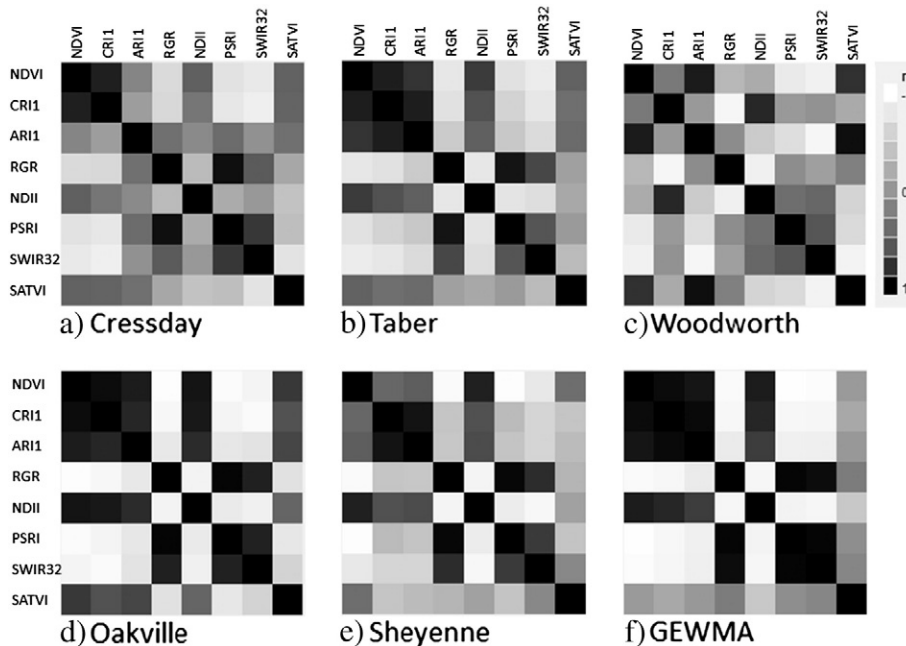
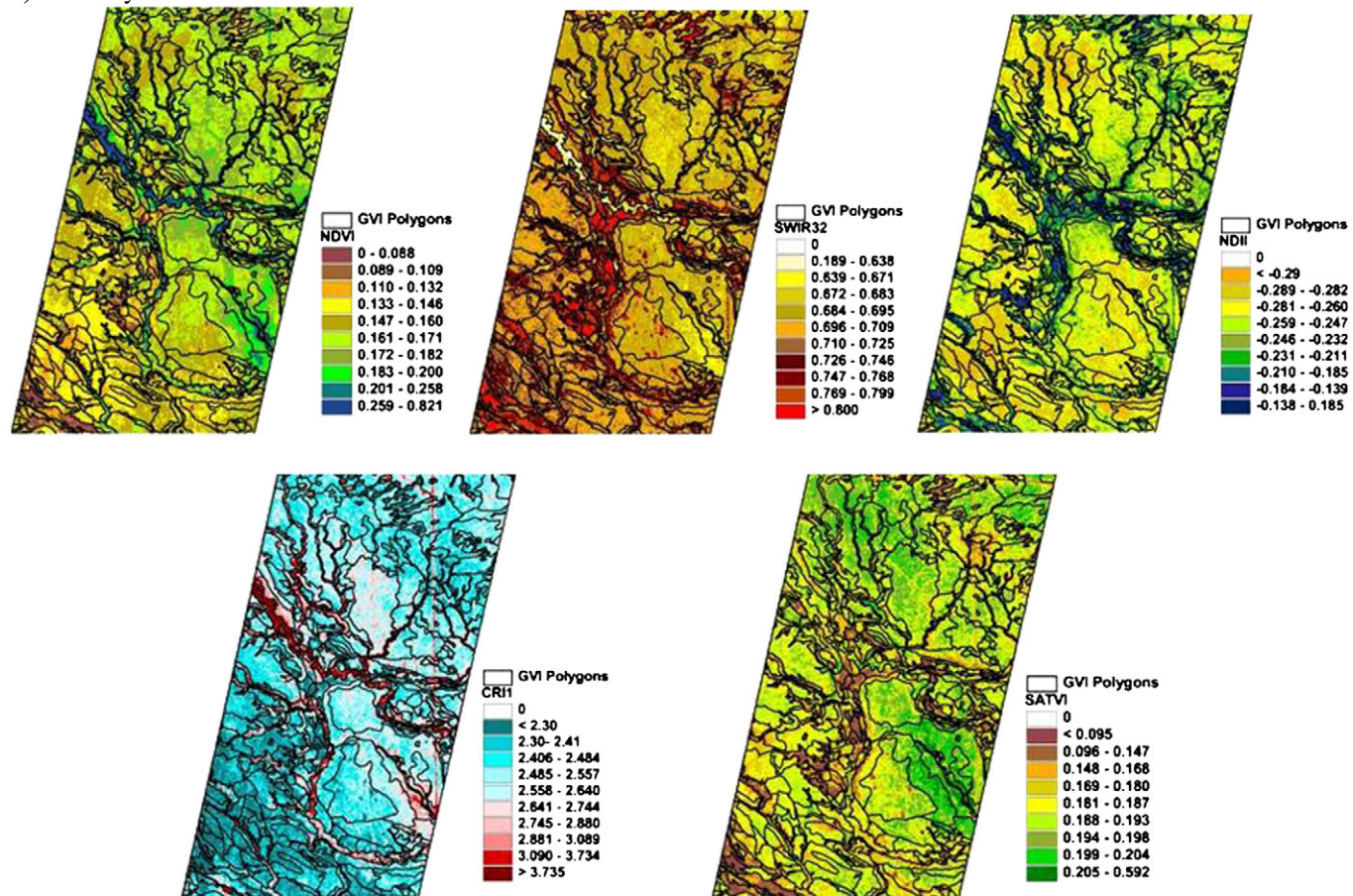
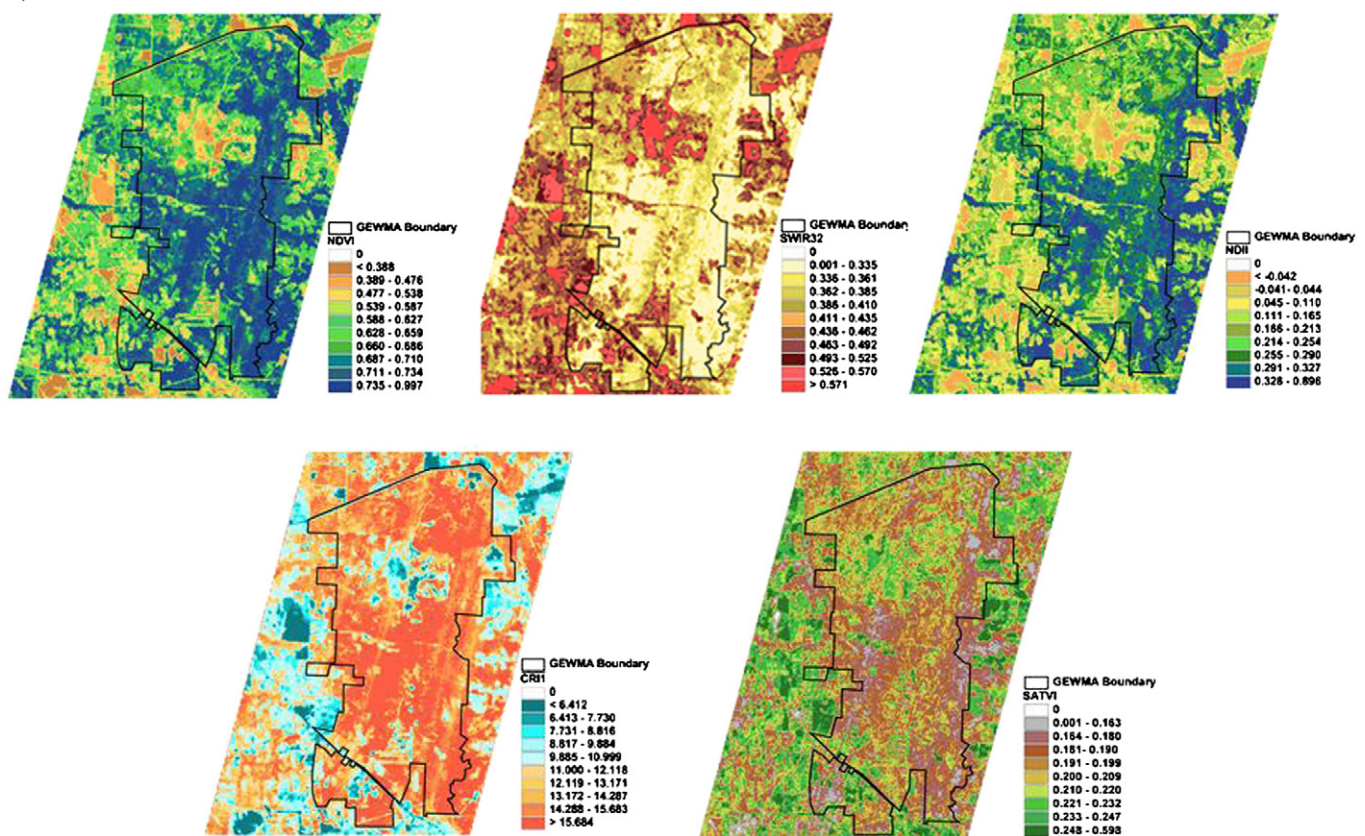


**Fig. 5.** Correlation maps for each study site for each vegetation index used in the analysis. a) Cressday; b) Taber; c) Woodworth; d) Oakville; e) Sheyenne; and f) GEWMA.

a) Cressday



b) GEWMA



## 4.2. Vegetation Index Suites as indicators: mean value approach

### 4.2.1. Alberta sites: GVI site types

For the two Alberta sites, their VI indicators are represented by frequency histograms of index values for dominant GVI site types (Fig. 7a, b). The histograms reveal that many GVI site types show a wide range of variation in individual index values, but that lentic, lotic, sandy, clay and blowout types have more distinct index profiles. The profiles are more distinct at the more xeric Cressday site than at more mesic Taber site (i.e., higher composition of low NDII values at Cressday than Taber). Among the GVI site types, it is notable that the clay and sandy types, which would be covered in grassland, show distinct differences. Among the indices, NDVI, SWIR32, and SATVI provide the most distinct profiles; these indices relate to fractional cover of PV, NPV and soil, and amount of herbage. The specific pigment indices reflect more of the presence of photosynthetic vegetation, and the NDII responds to moisture in vegetation or landscape and therefore is highly affected by micro-topography and woody vegetation.

The multivariate analysis of variance model to predict GVI site types from the suite of eight VIs was statistically significant for both sites (high degrees of freedom due to high polygon replication). However the contingency analysis of predicted versus expected GVI site types resulted in low  $R^2_u$  values and low Kappa values (Cressday produced notably better results than Taber) indicating that the model was not explaining variation well, and that agreement between predicted and expected GVI site types was low (Table 4). The low dynamic range of these most arid sites was also a contributing factor.

### 4.2.2. Sites in the USA: land cover classes

For the US sites, it was possible to examine the land cover types in a way that was more directly representative of an indicator of state change. The mean VI values for each land cover class are plotted as percentage deviation from the site mean with site mean values included for reference (Fig. 8). Since percentage deviation is greatly affected by the absolute magnitude of index values this approach does tend to enhance the apparent sensitivity of vegetation indices with inherently low absolute values. However, it did enable VI values with huge differences in value ranges to be plotted together as metric suites. The VI indicator suites reveal a significant amount of potential for discrimination among closely related land covers.

At Woodworth (Fig. 8a), there is huge variation in NDII which separates many land cover classes in terms of moisture content. There is significant variation in other index groups, but differences are more strongly grouped in well-defined classes such as green grassland and trees, dry or rank (stands dominated by culms and seed heads) grassland and agricultural fields or bare areas. This pattern is also evident for Oakville (Fig. 8b), but more significant variation is seen in the PSRI largely related to inactive agriculture and developed areas.

At SNG (Fig. 8c), the percentage deviation range was smaller than at the other sites, but the relativities between indices were different with variation in CRI1, ARI1, PSRI and SATVI the same or greater than that of NDII. Thus VI indicator suites can have differing sensitivities between geographical locations and land system conditions. Since this site was so wet in July 2011 (see site mean NDII), most variation was related to the intensity of signal from photosynthetic pigments (CRI1, ARI1, PSRI) and significant variation in SATVI which requires more study since this index was developed for arid grasslands.

At GEWMA (Fig. 8d), the VI indicator values for treed vegetation (invaded savanna, forest, red cedar and mesquite) were very similar, except for thickened oak woodlands (savanna). The site mean values were much closer to the tree signal at this site, thus the grassland areas exhibited the greatest deviation from site means. For these

vegetation classes, there was little difference between VI indicator suites for open or closed post oak stands and oak stands with significant evergreen invasion. However, pure red cedar and mesquite vegetation did exhibit a modestly different VI values to that of pure post oak.

The multivariate model to predict land cover classes from the suite of eight VIs was derived from the limited numbers of digitized vegetation class polygons at these sites. Nevertheless, models were statistically significant in all cases, and the  $R^2_u$  values indicated that the VI suite was about 80% successful in predicting the vegetation class (Table 4). However Kappa values only exceeded 0.8 at Woodworth and GEWMA. When the same analysis was applied to nominally assigned States, the model fits were significant only at Oakville and GEWMA, and the  $R^2_u$  and Kappa values were much lower (Table 4).

## 4.3. Vegetation Index Suites as indicators: pixel value distribution approach

From the preceding results, it was clear that effective use of VI suites as indicators of vegetation states required incorporation of more fine scale variation, and access to more descriptive metrics and statistics.

The frequency distribution histograms of vegetation indices for the selected polygons representing the states in Table 3 are shown in Fig. 9. The curves are color coded to match the color code in Table 3. Using an assumption of normality for all distributions, the Z statistics showed that pixel distributions of VI indicators (Fig. 9) were significantly different for most of the nominal states at each site, and for most of the individual VIs. Only a few paired comparisons revealed values <2.3 (not significant; Table 5), and these corresponded to logical responses. For example, at GEWMA, CRI1, PSRI and SATVI returned the same value distributions for woodland with red cedar and stands of red cedar. These kinds of responses are expected where VIs have low sensitivity to particular vegetation change. However these changes are picked up by other VIs in the indicator suite.

Visual assessment of pixel value histograms indicated that, there was little difference in the R1/R2 and D1 histograms at Cressday, but the D2 (badlands with a lot of bare ground) has a distribution that differs substantially in range of values. At Taber, the distributions show more variation in magnitude and shape between indices, with a useful contrast between NDVI and NDII. However, discrete differentiation was not evident for RGR, PSRI, SWIR32 or SATVI.

Visual assessment of histograms for Woodworth and Oakville showed that there is more noise in the distribution and more spread in the distributions for individual states (Fig. 9). The range of the overall site response is expanded by including inactive agriculture. Although, there are distinct differences in the range of the distributions between the R2/D1 and D2 states at Woodworth, the R1, R2 and D1 states have substantially overlapping index ranges at Oakville.

At Sheyenne, the distributions appeared to have very wide overlapping ranges of index values (Fig. 9). However, there were differences in the shapes indicating potential for identifying further discrete variation at finer scale. For example the SATVI had a range from 0 to 0.25 for the R2 state. In addition, the *Euphorbia/Poa* D2 area was more distinctly separated from the other states by the shape and location of the distribution for NDVI, PSRI and SWIR32.

Finally at GEWMA, whilst the pixel distribution for degraded grassland (D1) was visually distinctly different from the other states, the states with trees (and the tame pastures) had overlapping distributions (Fig. 9). However, although somewhat noisy, the distributions for ARI1 and CRI1 do visually separate the invasive red cedar D2 state from the other treed states. In this treed landscape, SWIR32 and SATVI would not be expected to be discriminatory for the treed states as they are designed to be sensitive to herbaceous fractional cover and biomass. Nevertheless, it is notable that although

**Fig. 6.** Maps showing the spatial pattern of five vegetation indices calculated for simulated Sentinel 2 imagery for a) the semi-arid mixed prairie (Cressday); and b) the post oak savanna (GEWMA); the study sites representing the two extremes of the continental transect.

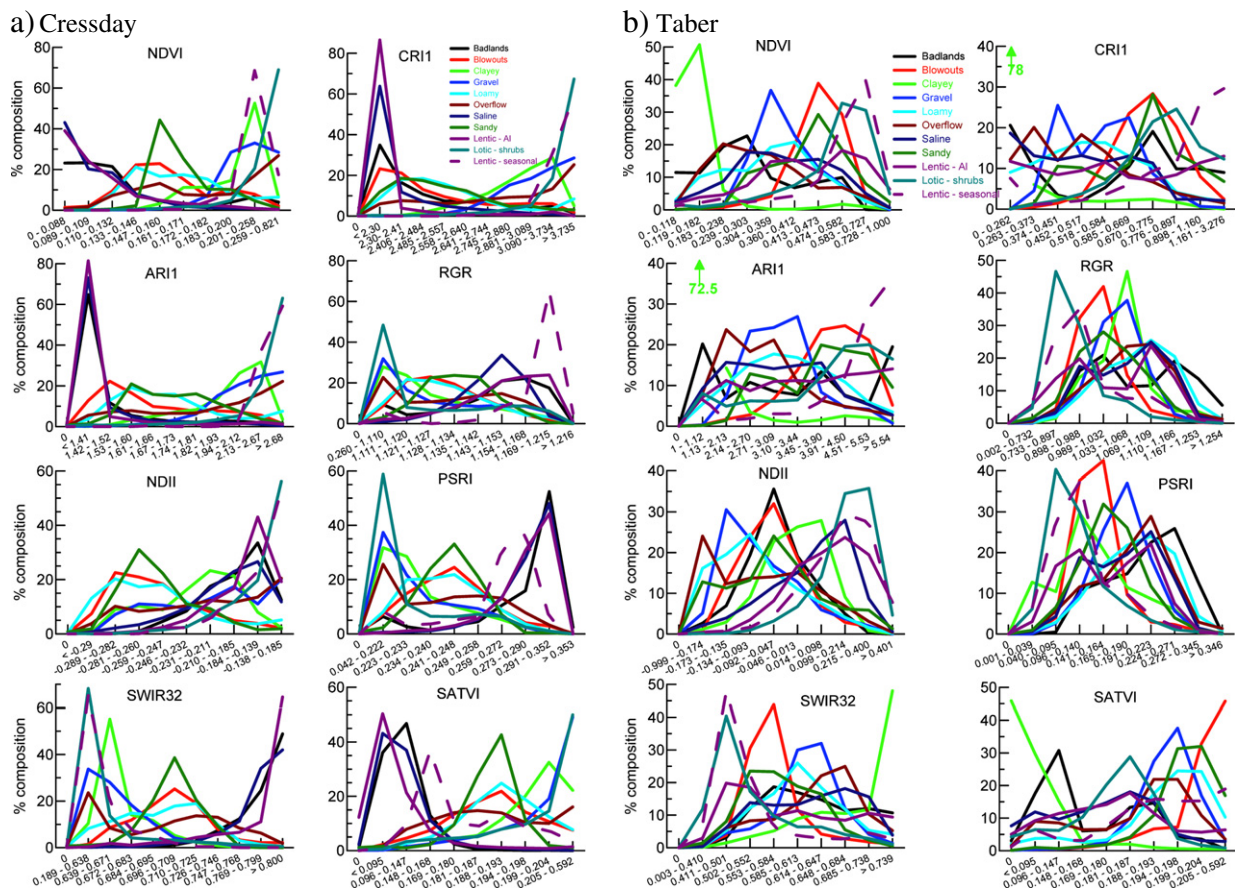


**Fig. 7.** Distributions of vegetation index values among the GVI site types for polygons where a single type occupies >67% of the area: a) Cressday; and b) Taber.

overlapping, small discrete shifts in the distributions of SATVI were visibly evident for the D2-R2-R1-R2-D1 sequence corresponding to red cedar–post oak with red cedar–flooded forest–thickened post oak–degraded grassland. The sequence corresponds to a gradient of increased openness of canopies to reveal understory.

#### 4.4. Scaling analysis with MODIS and VIIRS

The seasonal variation in vegetation phenology and spectral properties present in virtually all savanna and grassland systems indicates

the need for temporal variation to be incorporated into development of indicators of vegetation state. The analysis presented in this study is constrained by the single date mid-late summer timing of images used. Therefore, it was important to examine the potential for scaling this suite of indices to MODIS and VIIRS.

The relationships between vegetation indices from simulated MODIS or simulated VIIRS and simulated Sentinel 2 data fall into several groups (Table 6): excellent  $R^2$  with near 1:1 slopes—NDVI, NDII, PSRI; excellent  $R^2$  and slopes less than 1:1—SWIR32, SATVI; excellent  $R^2$  and slopes greater than 1:1—RGR and NDVI at Sheyenne and GEWMA; and poor

**Table 4**

Results of fitting a multivariate model using the eight vegetation indices to predict land cover classes (corresponding to those shown in Figs. 6 and 7) and nominally assigned vegetation states described in Fig. 1 (note: the latter was not applied to the Alberta sites as there is insufficient information on vegetation condition to attempt to define States other than for illustration purposes). The table shows the significance of the whole model (Wilks' Lambda) and then the results of a contingency analysis comparing predicted class or state from the model and actual class or state.  $R^2_u$  is the proportion of uncertainty explained by the model fit. The Likelihood Ratio  $\chi^2$  tests whether the predicted and expected are the same in each class category. The Kappa statistic tests the strength of agreement between predicted and expected; values less than 0.8 generally indicate an unsatisfactory agreement.

Site	Classification	Manova model		Contingency analysis					
		Wilks' Lambda	Prob > F	N	Df	$R^2_u$	$\chi^2$	Prob > $\chi^2$	Kappa
<b>Land cover classifications</b>									
Cressday	GVI site type	0.0338	<0.0001***	220	49	0.438	364.03	<0.0001***	0.51
Taber	GVI site type	0.4539	<0.0001***	1440	529	0.206	1549.7	<0.0001***	0.123
Woodworth	Veg Class	0.00001	0.0011***	20	64	0.869	68.91	0.315	0.826
Oakville	Veg Class	0.00053	<0.0001***	31	81	0.82	106.14	0.032*	0.709
Sheyenne	Veg Class	0.00035	0.0061**	33	196	0.781	122.6	1.000	0.641
GEWMA	Veg Class	0.00003	<0.0001***	29	100	0.852	107.04	0.2968	0.801
<b>Nominal vegetation states</b>									
Woodworth	States	0.1453	NS	20	9	0.614	29.27	0.0006***	0.711
Oakville	States	0.0752	0.0293*	31	25	0.717	68.75	<0.0001***	0.733
Sheyenne	States	0.239	NS	33	16	0.345	29.87	0.0187*	0.345
GEWMA	States	0.1325	0.0082**	29	9	0.547	37.88	<0.0001***	0.653

\* significant at  $P > 0.05$ ; \*\* significant at  $P > 0.01$ ; \*\*\* significant at  $P > 0.001$ .

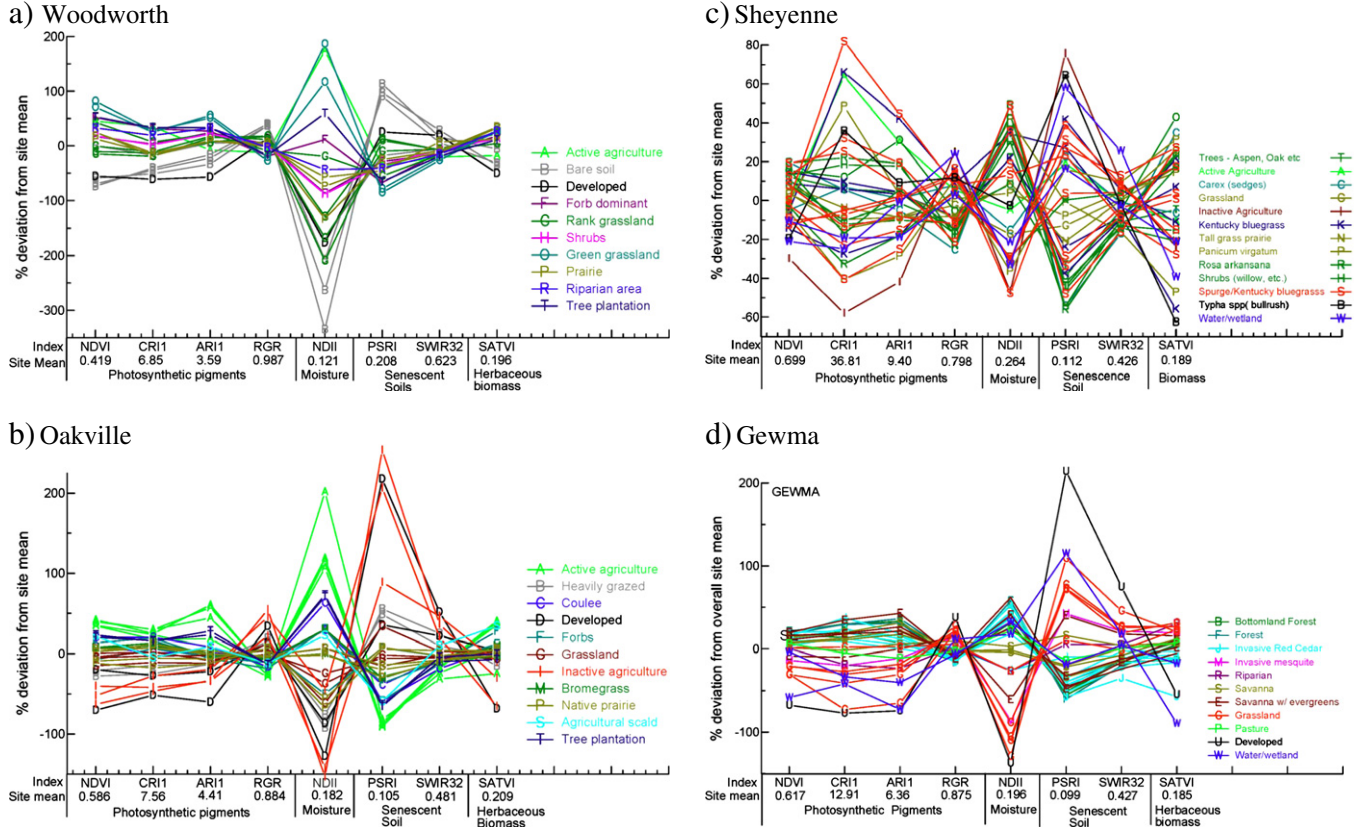


**Fig. 8.** VI indicators for sample polygon areas shown in Fig. 4 aggregated to composite land cover classes on the basis of local land use and the aerial photo classifications (i.e., grazed paddocks, riparian (coulee) areas, conserved grasslands, areas known to be under specific jurisdiction such as School Trust land, National Wildlife Refuges etc.). a) Woodworth; b) Oakville; c) Sheyenne; and d) GEWMA.

$R^2$ —psARI. The relationship between MODIS or VIIRS indices and Sentinel indices over all sites is close to 1:1 for NDVI and NDII (Table 6). However, although the relationship is good for SWIR32, the slope is much less than 1:1 and  $R^2$  is low for the Woodworth site (Table 6; Fig. 10). Standard deviations of Sentinel values in the mid-ranges of NDVI and NDII, and towards the upper range of SWIR32 are quite high. Standard deviations rise with increase index values for SWIR32, NDII and CRI1, but decline with increasing values for SATVI. The results emphasized that there is no simple surrogate wavelength for MODIS and VIIRS that can substitute for the 700 nm band needed to calculate the ARI1. There were also significant differences in relationships between sites, with Woodworth (latest image date, low dynamic range over grassland, and areas of open water present) having relatively poor  $R^2$  for SWIR32, NDII, psARI1 and CRI1.

Regressions between vegetation indices from simulated VIIRS and MODIS and mean indices from simulated Sentinel 2 data are similar and comparable despite the much larger coverage of a VIIRS pixel (Table 6). Notable variation between MODIS and VIIRS occurs for vegetation indices where spectral bands differ markedly with Sentinel 2 (see Table 1). This particularly affects the SWIR32 and NDII indices since there is a 30 nm difference in band center for the SWIR band used in these indices. There is also a significant difference in the band centers for the red and green bands used in calculation of RGR and PSRI.

Comparison of VI values between simulated MODIS, VIIRS and Sentinel 2 for selected vegetation polygons that relate to important vegetation states at GEWMA (see Table 3) showed that MODIS and VIIRS still retrieve clear differences in values for some vegetation states (Table 7). In addition, where values for one index were similar between types, a difference was evident in another index suggesting that combinations of indices can be effectively used.

However, the lower pixel resolution for VIIRS, which results in more contamination of the signature from adjoining vegetation, especially for small polygons, does result in smaller differences. On the other hand, VIIRS and MODIS index values clearly reflect differences between vegetation states with larger sampling areas observed in the simulated Sentinel 2 data. Both VIIRS and MODIS data capture sufficient variation for one moment in time to suggest that full temporal sequences of either MODIS or VIIRS combined with Sentinel 2 data have very significant potential for enhanced discrimination among natural vegetation types through definition of sub-pixel composition and spectral unmixing from Sentinel 2 end members.

## 5. Discussion

This analysis has shown that the Sentinel 2 sensor could provide a suite of vegetation indices that together can act as indicators of vegetation states in grassland and savannas. These indicators could inform the Ecological Site Description framework being implemented by the USDA NRCS. The analysis examined approaches based on mean values for target land types or management units, and based on pixel value distributions within these units that reveal more detail about vegetation condition. Although the degree of discrimination obtained between vegetation states was somewhat constrained by the limited range of spectral variation found in herbaceous vegetation at some sites, most pixel value distributions proved to be significantly different based on a liberal application of the Z statistic test. In addition, the models derived from the mean value approach show potential for state discrimination that could be markedly enhanced by the use of multi-date imagery that captures phenological variation throughout the growing seasons. It is evident from this study that the timely assessments and availability of time series of vegetation indices are essential to create more definitive

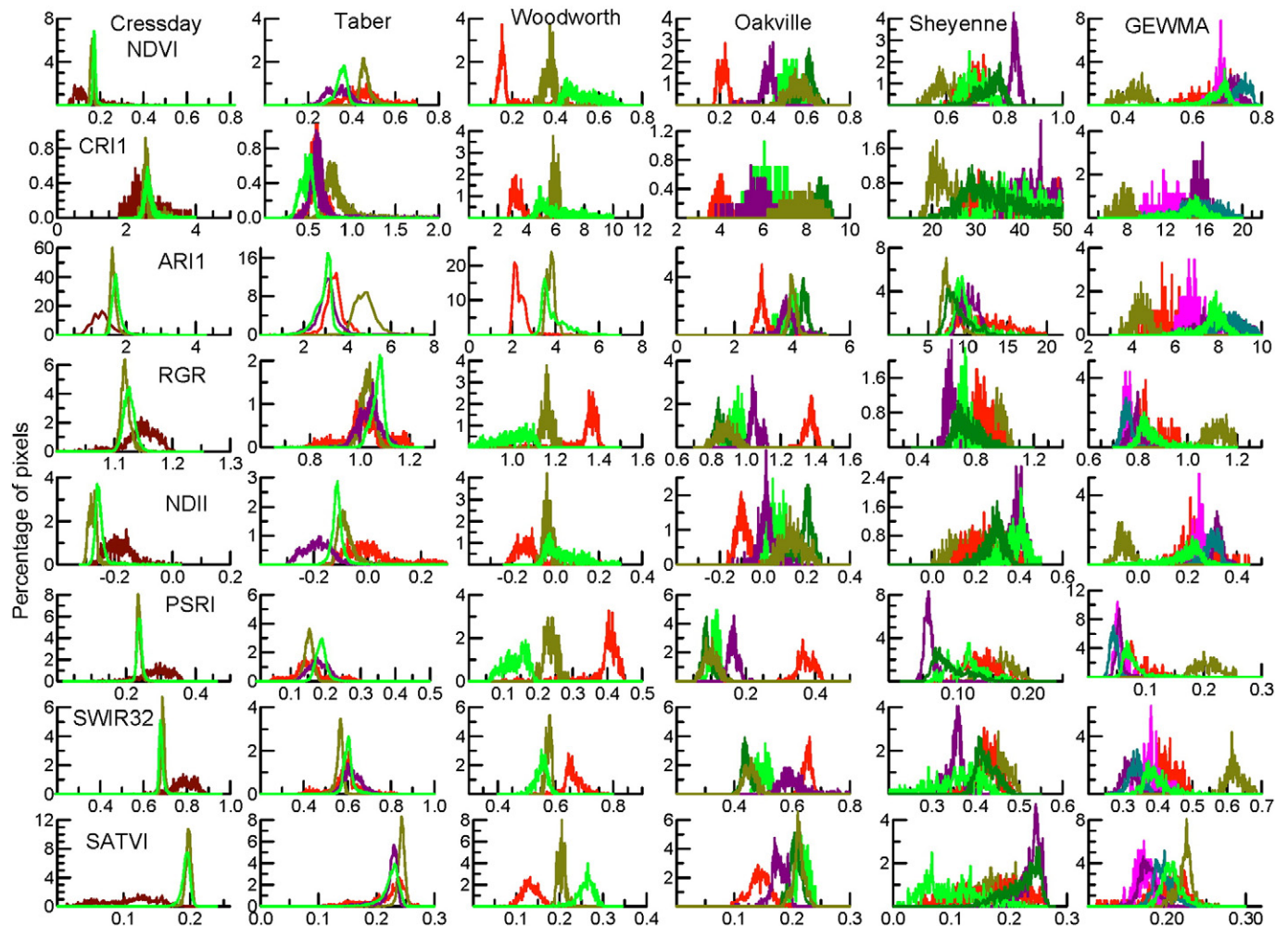


**Fig. 9.** Distributions of pixels from study site nominally representing reference, degraded and converted states (Fig. 1 and Table 4) plotted on a continuum for each vegetation index from simulated Sentinel 2 data. Cressday (R1/2—grassland on loam; D1—blowout grassland; D2—badlands; C—tame pasture). Taber (R1/2—grassland on loam; D1—blowout grassland; D2—badlands; C—agriculture). Woodworth (R1/2—school trust grassland; D2—bromegrass; C—agriculture). Oakville Prairie (R1—saline grassland; R2—School Trust Land; D1—grassland; D2—heavily grazed paddocks; C—agriculture). Sheyenne (R1—Viking Prairie; R2—*Panicum virgatum*/Carex spp; D1—*Panicum virgatum*/Poa pratense; D2—*Euphorbia esula*/Poa pratense; C—agriculture). GEWMA (R1—renovated *Quercus stellata*/*Schizachyrium scoparium*; R2—*Quercus stellata* woodland; D1—*Quercus stellata*/*Juniperus virginiana*; D1—*Schizachyrium scoparium*/*Ilex vomitoria*/*Juniperus virginiana*/bare ground; D2—*Juniperus virginiana* stands; C—tame pasture).

state indicators that capture the combined phenological and spatial differences needed to discriminate among grassland and savanna vegetation states. For example, in TX, the late summer timing of imagery used here enhanced the contrast between tree canopy densities for forest and savanna and hence visibility of dry grass understory. However, this was the least ideal timing for detection of evergreen invasion of deciduous savanna woodland, and the contrast between evergreen invasive

species and deciduous native trees is minimized. Winter imagery when deciduous canopies are absent is needed to optimize detection of degraded states involving evergreen invasion. Sites where local factors reduced discriminatory sensitivity of VI suites, such as seasonal wet conditions delaying development of naturally occurring landscape gradients in VI values (SNG), and relatively mixed grassland principally occupying D1/D2 states (Woodworth), emphasized that multi-date analysis will be really important, and that some grasslands are just similar.

Although the red edge has been the subject of substantial study and development of a great diversity of indices beyond the NDVI (e.g., Elvidge and Chen, 1995), including for the Sentinel 2 and 3 missions (Clevers & Gitelson, 2012), other absorption regions have been less well explored, at least with multi-spectral data. The water absorption bands at 1200–1300 and 1600–1700 nm have received attention (e.g., Fensholt & Sandholt, 2003; Gao, 1996; Hardisky et al., 1983) and direct retrieval of equivalent water thickness has been explored (e.g., Ferreira et al., 2011; Yilmaz, Hunt, & Jackson, 2008). However, the potential sensitivities that may be addressed with the combination of SWIR bands at 1600–1700 nm and 2000–2200 nm have been little explored, with soils in particular being largely ignored as a target (this being a recent exception, Summers et al., 2011). Given the attention paid to the development of so many variants of vegetation indices, it is surprising that so little attention has been paid to the application of

**Table 5**

Ranges of values for the Z statistic for two way comparison of pixel distributions of vegetation indices for individual state polygons shown in Fig. 9 along with listing of nominal vegetation states that were not significantly different for each vegetation index. The analysis uses each pixel as an observation, hence large pixel counts increase sensitivity.

Site	Range in Z statistic (significant Z > 2.3)	Paired comparisons that were NOT significant Z < 2.3
Cressday	3.03–77.9	None
Taber	2.44–> 1000	None
Woodworth	5.43–138.7	D1 versus R2 for CRI1
Oakville	8.77–307.6	None
Sheyenne	3.14–137.7	C1 versus R2 for NDVI; D2 versus R2 for SWIR32; D1 versus C1 for SATVI
GEWMA	4.75–211.2	D1 versus D2 for CRI1, PSRI, and SATVI; D2 versus C1 for NDII; R1 versus D2 for RGR; R1 versus C1 for RGR

**Table 6**

Slope and  $R^2$  for regression relationships between vegetation indices from simulated MODIS and VIIRS data, and mean values for indices from simulated Sentinel 2 data.

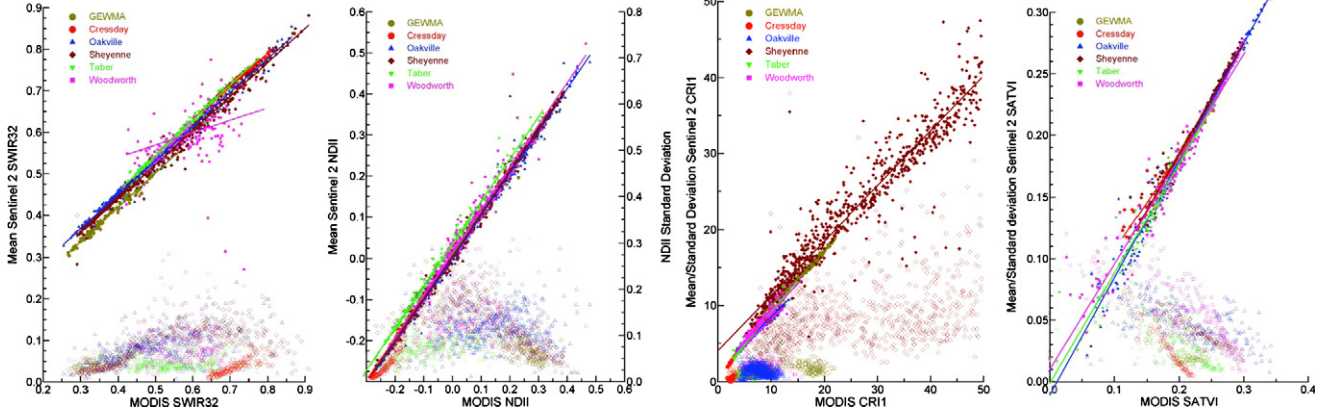
Index	Cressday		Taber		Oakville		Woodworth		Sheyenne		GEWMA	
	Slope	$R^2$	Slope	$R^2$	Slope	$R^2$	Slope	$R^2$	Slope	$R^2$	Slope	$R^2$
<i>VIIRS</i>												
NDVI	0.94	0.95	0.98	0.99	0.99	0.99	0.86	0.91	1.04	0.99	1.03	0.99
SWIR32	1.01	1.0	1.09	0.98	1.04	0.97	0.35	0.12	1.02	0.99	1.07	0.98
NDII	1.03	0.99	1.01	0.99	0.98	0.99	1.15	0.77	0.99	0.98	0.99	0.99
psARI1	−0.48	0.08	−0.48	0.21	−0.20	0.26	0.55	0.35	−0.53	0.73	−0.28	0.70
CRI1	1.01	0.97	0.84	0.98	0.63	0.89	0.69	0.79	0.72	0.95	0.73	0.99
PSRI	0.86	1.00	0.94	1.00	0.94	0.99	0.94	0.98	0.97	0.99	0.94	0.99
RGR	1.00	0.98	0.88	0.99	0.80	0.99	0.87	0.98	0.83	0.99	0.83	0.99
SATVI	0.87	0.94	0.91	0.98	0.90	0.98	0.87	0.96	0.88	0.88	0.96	0.98
<i>MODIS</i>												
NDVI	1.02	0.99	1.03	0.99	1.10	0.99	1.03	0.96	1.10	1.00	1.12	0.98
SWIR32	0.80	0.98	0.85	0.98	0.82	0.99	0.30	0.11	0.82	0.99	0.82	0.99
NDII	1.07	0.99	1.03	0.99	1.03	0.99	1.03	0.96	1.02	0.99	1.00	0.99
psARI1	−0.05	0.00	0.36	0.16	−0.07	0.02	0.87	0.39	−0.72	0.57	−0.37	0.61
CRI1	1.03	0.98	0.85	0.98	0.69	0.96	0.79	0.94	0.72	0.95	0.72	0.98
PSRI	0.92	0.99	0.96	1.00	0.94	0.99	0.96	0.98	0.98	1.00	0.95	0.99
RGR	1.20	0.99	1.07	0.99	1.04	0.99	1.09	0.99	1.02	0.99	0.99	0.97
SATVI	0.77	0.94	0.89	0.97	0.95	0.98	0.85	0.96	0.90	0.97	0.89	0.98

these in concert for practical management and monitoring. However, with the absence of any global coverage of hyperspectral data for the next 10 years, and very limited potential from narrow swath sensors in planning, there is a need to harness the multivariate potential of global multispectral imaging from Sentinel 2 and Landsat.

Most of the vegetation indices calculable with Sentinel 2 were scalable to MODIS and VIIRS. Although the coarse spatial greatly limits patch

detection, these indices show individual differences among important grassland and savanna vegetation types even at 500 and 750 m scale. There was significant variation in Sentinel 2 values for a given MODIS or VIIRS value. Sub-pixel characterization and end-member definition with Sentinel 2 can untangle this variation. In addition, application of reflectance fusion models such as STARFM (Hilker et al., 2009) with MODIS, VIIRS and Sentinel 3 can further enhance the time series of Sentinel 2

### a) Sentinel 2 vs MODIS



### b) Sentinel 2 vs VIIRS

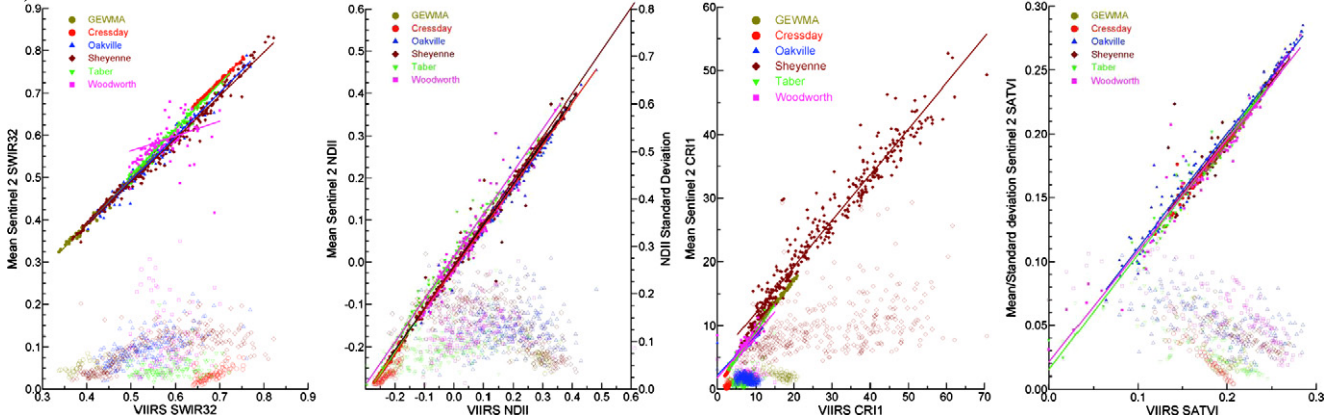


**Fig. 10.** Relationships between the mean (closed symbol) and standard deviation (open symbol) of SWIR32, NDII and CRI1 and SATVI calculated from simulated Sentinel 2 data and the corresponding mean calculated from a) simulated MODIS data; and b) simulated VIIRS data.

**Table 7**

Comparison of vegetation index values (with standard deviations) retrieved for simulated Sentinel 2, MODIS and VIIRS data for selected example vegetation polygons representing certain major vegetation types at GEWMA. Neither MODIS nor VIIRS provides a surrogate for the ARI1.

State	Sensor	NDVI	CRI1	ARI1	RGR	NDII	PSRI	SWIR32	SATVI
GEWMA									
Post oak savanna									
Schizachyrium scoparium degraded grassland (D1)	V	0.565 ± 0.043	11.3 ± 1.53	NA	1.04 ± 0.04	0.055 ± 0.040	0.157 ± 0.022	0.513 ± 0.042	0.224 ± 0.002
	M	0.540 ± 0.006	9.88 ± 0.13	NA	1.04 ± 0.002	-0.001 ± 0.009	0.201 ± 0.003	0.550 ± 0.016	0.238 ± 0.001
	S2	0.493 ± 0.066	9.42 ± 1.75	5.21 ± 0.82	1.05 ± 0.076	-0.004 ± 0.062	0.167 ± 0.039	0.554 ± 0.060	0.222 ± 0.015
Quercus stellata woodland—thickened (R2)	V	0.676 ± 0.024	15.5 ± 1.18	NA	0.90 ± 0.05	0.192 ± 0.031	0.097 ± 0.015	0.425 ± 0.020	0.210 ± 0.008
	M	0.679 ± 0.027	15.4 ± 1.25	NA	0.88 ± 0.038	0.171 ± 0.048	0.120 ± 0.016	0.391 ± 0.031	0.224 ± 0.010
	S2	0.655 ± 0.058	14.1 ± 1.80	7.49 ± 0.84	0.87 ± 0.071	0.188 ± 0.075	0.085 ± 0.029	0.409 ± 0.047	0.203 ± 0.015
Quercus stellata/Juniperus virginiana-invaded woodland (D1)	V	0.752 ± 0.001	20.2 ± 0.06	NA	0.78 ± 0.007	0.317 ± 0.006	0.063 ± 0.002	0.345 ± 0.008	0.189 ± 0.004
	M	0.728 ± 0.030	18.5 ± 2.43	NA	0.83 ± 0.044	0.263 ± 0.040	0.099 ± 0.016	0.324 ± 0.040	0.210 ± 0.011
	S2	0.705 ± 0.055	16.4 ± 2.60	8.22 ± 1.13	0.82 ± 0.072	0.281 ± 0.074	0.067 ± 0.028	0.349 ± 0.057	0.185 ± 0.018
Flooded Bottomland Forest (R1)	V	0.759 ± 0.004	18.3 ± 0.33	NA	0.76 ± 0.015	0.318 ± 0.014	0.052 ± 0.004	0.354 ± 0.011	0.193 ± 0.006
	M	0.755 ± 0.008	18.4 ± 0.72	NA	0.77 ± 0.013	0.293 ± 0.017	0.075 ± 0.004	0.301 ± 0.014	0.208 ± 0.006
	S2	0.739 ± 0.026	16.1 ± 1.23	8.18 ± 0.65	0.75 ± 0.030	0.303 ± 0.040	0.044 ± 0.011	0.340 ± 0.030	0.191 ± 0.014

and LANDSAT 8 (e.g., Schmidt et al., 2012). Appropriate spectral downscaling that retains radiometric quality would obviate the need for downscaling of vegetation indices; all VI indicators and VI indicators time series may then be calculated from enhanced LANDSAT 8 and Sentinel 2 scale data. The much enhanced imaging frequency can deliver particular benefits in cloudy northern grassland regions, and tropical savannas with significant cloudiness pre- and post-monsoon.

The pixel value distribution approach presented here provides the opportunity to use a variety of statistical distribution metrics to characterize vegetation states in the grassland–savanna continuum. Since the Z statistic approach treats pixels as samples of a distribution, it is a fairly liberal test of differences. In addition, it is not valid for highly skewed distributions. However, it is quite likely that a highly skewed pixel distribution in one target polygon will have a markedly different median values, and measures of skewness and kurtosis, compared to another polygon. Therefore a combination of the Z statistic test and other descriptive statistics for distributions could form the basis for metrics of state change.

The results here are sufficient to form the basis for a framework that could be applied to assist the monitoring of vegetation states with the NRCS ESD approach using multi-temporal Sentinel 2 (supplemented with Landsat 8) imagery. Such a framework would be based on the following procedure.

1. Defining “typical” calibration sites for vegetation representative of R1, R2, D1, D2 and C1 states within ESD regions.
2. Define a set of overlapping phenological periods for each growing season, probably based on some objective rules about the combined day length, moisture and temperature conditions and anchored to a rule defining the start of the growing season.
3. Undertake comprehensive testing and assessment to establish robust detection limits for identification of states. For example, it may be much easier to detect states that are characterized by changes in fractional cover of woody vegetation, herbaceous vegetation and soil, than to detect differences in composition of mesic grasslands that define states D1 and D2.
4. Establishing baseline temporal metric suites for each state, i.e., a set of mean values and distribution shapes for each phenological period.
5. Use established (e.g. Guerschman et al., 2009) or new approaches to derive baseline temporal values for fractional cover of PV, NPV and bare ground to complement the VI suites.
6. Establish a set of thresholds made up of multiple metrics derived from the statistical properties of the pixel value distributions such as mean, median, skewness, kurtosis and other moments. The

kinds of changes in VI pixel distributions that could define state change are shown in Fig. 11. For example, the mean value may shift without a change in shape; the mean value may stay the same but the spread may increase; both the spread and mean may change; or the distribution may change to bimodal indicating patch development. The Z statistic can be used to test differences between normal or near-normal distributions.

7. Implement a change detection system based on detecting shifts in the properties of VI indicators from year to year.

In the procedure outlined above, thorough testing and analysis of critical seasonal timings for image acquisition for each ecosystem–climate combination is essential to define the minimum temporal date and frequency of image acquisition required for state detection in any system.

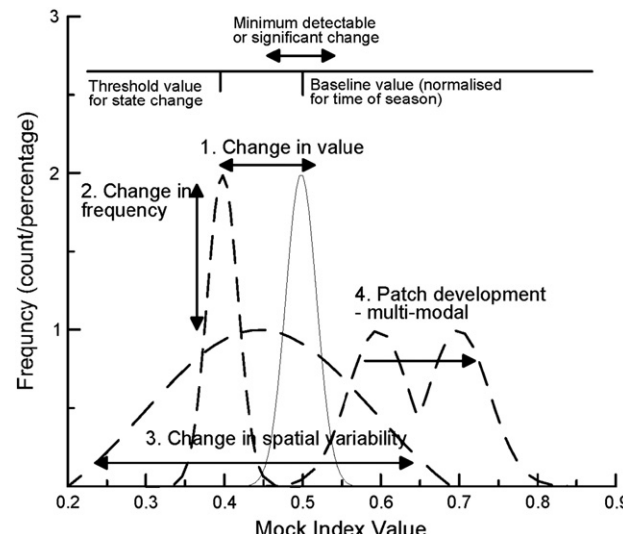


**Fig. 11.** Conceptual basis for establishing a monitoring program to detect state changes in natural lands based on suites of vegetation indices from Sentinel 2. The approach requires establishment of a baseline set of VI indicators including spatial distribution characteristics for a set of key seasonal phenological dates. Subsequent monitoring would examine changes in the VI indicators in terms of: 1. Changes in mean values past a threshold for state change; 2. Changes in frequency counts/percentages; 3. Changes in the width of the distribution indicating increased variability; and 4. occurrence of multi-modalities indicating development of distinct patches.

## 7. Conclusion

This analysis has indicated that suites of vegetation indices calculated from spectral bands offered by the proposed Sentinel 2 sensors could provide individual and composite indicators of vegetation states in grassland and savannas. The approach used here showed that analysis of distributions of pixels as individual observations for target areas allows for finer distinctions between vegetation conditions that might improve detection of vegetation states as defined in real-world S&T models. They also demonstrated the value of utilizing indices with sensitivity to key properties and functional attributes of vegetation, beyond the red edge. However, lower sensitivity at some sites, partially due to seasonal conditions or predominantly degraded vegetation types, suggests that time series of index suites may be needed for fully effective applications. A procedure for developing a monitoring system for grassland and savanna vegetation states and transitions was proposed based on VI suites from optical imagery with high temporal frequency. This system would form part of a more comprehensive approach that might utilize high resolution imagery to scale demographic changes in woody plant densities and herbaceous patch structures (e.g., Bestelmeyer, Trujillo, Tugel, & Havstad, 2006) to the spectral domain provided by the Sentinel 2/Landsat sensor class. Practical application of this approach must include multiple metrics of index profiles in space and time including changes in the pixel value distribution shapes and properties within target land units. All indices except ARI1 were scalable to MODIS and VIIRS spectral bands enabling the use of reflectance fusion models to enhance Sentinel 2 time series. The free Landsat archive, enhanced radiometric resolution from new Sentinel 2 and LANDSAT 8 sensors and the much reduced revisit times promised by combination of Sentinel 2 and Landsat data should provide global time series at 20–30 m pixel resolution and revolutionized the monitoring and modeling potential in grasslands and savannas (Drusch et al., 2012; Hansen & Loveland, 2012; Wulder, Masek, Cohen, Loveland, & Woodcock, 2012). Further work is needed to characterize the potential benefits and practical operational programs possible from state indicators based on time series of Sentinel 2 and Landsat vegetation indices.

## Acknowledgments

This research was partially supported by grants from NASA (Contract #NNX09AQ81G and #NNX10AH20G) and the Canadian Space Agency (GRIP IMOU No: 08MOA84819). I thank the Resource Information Management Branch of Sustainable Resource Development, Alberta for providing access to the Grassland Vegetation Inventory.

## References

- Adams, B. W., Ehler, R., Moisey, D., & McNeil, R. L. (2003). *Rangeland plant communities and range health assessment guidelines for the foothills fescue natural subregion of Alberta*. Lethbridge: Rangeland Management Branch, Public Lands Division, Alberta Sustainable Resource Development (Pub. No. T/038 85 pp.).
- Adams, B. W., Poulin-Klein, L., Moisey, D., & McNeil, R. L. (2004). *Rangeland plant communities and range health assessment guidelines for the mixedgrass natural subregion of Alberta*. Lethbridge: Rangeland Management Branch, Public Lands and Forests Division, Alberta Sustainable Resource Development (Pub. No. T/03940 101 pp.).
- Adams, B. W., Poulin-Klein, L., Moisey, D., & McNeil, R. L. (2005). *Rangeland plant communities and range health assessment guidelines for the dry mixedgrass natural subregion of Alberta*. Lethbridge: Rangeland Management Branch, Public Lands Division, Alberta Sustainable Resource Development (Pub. No. T/040 106 pp.).
- Agresti, A. (1990). *Categorical data analysis*. New York: John Wiley and Sons, Inc.
- Anderson, R. C. (1983). The eastern prairie-forest transition—An overview. In Brewer Richard (Ed.), *Proceedings of the Eighth North American Prairie Conference* (pp. 86–89). Kalamazoo, Michigan: Department of Biology, Western Michigan University (1–4 August 1982).
- Anyamba, A., & Tucker, C. J. (2005). Analysis of Sahelian vegetation dynamics using NOAA AVHRR NDVI data from 1981–2003. *Journal of Arid Environments*, 63, 596–614.
- Apan, A., Held, A., Phinn, S., & Markley, J. (2004). Detecting sugarcane 'orange rust' disease using EO-1 Hyperion hyperspectral imagery. *International Journal of Remote Sensing*, 25, 489–498.
- Ash, A. S. J., Bellamy, J. A., & Stockwell, T. G. H. (1994). State and transition models for rangelands. 4. Application of state and transition models to rangelands in Northern Australia. *Tropical Grasslands*, 28, 223–228.
- Asner, G. P., & Heidebrecht, K. B. (2002). Spectral unmixing of vegetation, soil and dry carbon cover in arid regions: Comparing multispectral and hyperspectral observations. *International Journal of Remote Sensing*, 23, 3939–3958.
- Asner, G. P., & Heidebrecht, K. B. (2003). Imaging spectroscopy for desertification studies: Comparing AVIRIS and EO-1 Hyperion in Argentina drylands. *IEEE Transactions on Geoscience and Remote Sensing*, 41, 1283–1296.
- Asner, G. P., & Lobell, D. B. (2000). A biogeophysical approach for automated SWIR unmixing of soils and vegetation. *Remote Sensing of Environment*, 74, 99–112.
- Bastin, G. N., Ludwig, J. A., Eager, R. W., Chewings, V. H., & Liedloff, A. C. (2002). Indicators of landscape function: Comparing patchiness metrics using remotely-sensed data from rangelands. *Ecological Indicators*, 1, 247–260.
- Bellamy, J. A., & Brown, J. R. (1994). State and transition models for rangelands. 7. Building a state and transition model for management and research on rangeland. *Tropical Grasslands*, 28, 247–255.
- Bestelmeyer, B. T., Goolsby, D. P., & Archer, S. R. (2011). Spatial perspectives in state and transition models: A missing link to land management? *Journal of Applied Ecology*, 48, 746–757.
- Bestelmeyer, B. T., Trujillo, D. A., Tugel, A. J., & Havstad, K. M. (2006). A multi-scale classification of vegetation dynamics in arid lands: What is the right scale for models, monitoring and restoration? *Journal of Arid Environments*, 65, 296–318.
- Briske, D. D., Fuhlendorf, S. D., & Smeins, F. E. (2005). State-and-transition models, thresholds and rangeland health: A synthesis of ecological concepts and perspectives. *Range Ecology and Management*, 58, 1–10.
- Burkinshaw, A. M., Willoughby, M. G., France, K., Loonen, H., & McNeil, R. L. (2009). *Rangeland plant communities and range health assessment guidelines for the central parkland subregion of Alberta*. Red Deer: Rangeland Management Branch, Public Lands Division, Alberta Sustainable Resource Development (Pub. No. T/125 195 pp.).
- Cathey, J. C., Mitchell, D. R., Prochaska, B., DuPree, D. F., & Sosebee, S. R. (2006). Managing Yaupon in the Post Oak Savannah. *Rangelands*, 28, 24–27.
- Clevers, J. G. P. W., & Gitelson, A. A. (2012). Remote estimation of crop and grass chlorophyll and nitrogen content using red-edge bands on Sentinel-2 and -3. *International Journal of Applied Earth Observation and Geoinformation*, 23, 344–351.
- Conner, R., Seidl, A., VanTassel, L., & Wilkins, N. (2001). *United States grasslands and related resources: An economic and biological trends overview*. College Station, Texas: Texas Cooperative Extension Reports and Publications (154 pp.).
- Datt, B., & Jupp, D. L. B. (2004). *Hyperion Data Processing Workshop: Hands-on processing instructions*. Canberra: CSIRO.
- Datt, B., McVicar, T. R., Van Niel, T. G., Jupp, D. L. B., & Pearlman, J. S. (2003). Preprocessing EO-1 Hyperion hyperspectral data to support the application of agricultural indexes. *IEEE Transactions on Geoscience and Remote Sensing*, 41, 1246–1259.
- Drusch, M., Del Bello, U., Carlier, S., Colin, O., Fernandez, V., Gascon, F., et al. (2012). Sentinel-2: ESA's optical high-resolution mission for GMES operational services. *Remote Sensing of Environment*, 120, 25–36.
- Drusch, M., Gascon, F., & Berger, M. (2010). *GMES Sentinel-2 Mission Requirements Document. Issue 2 revision, EOP-SM/1163/MR-dr*. : European Space Agency (38 pp.).
- Elvidge, C. D., & Chen, Z. (1995). Comparison of broad-band and narrow-band red and near-infrared vegetation indices. *Remote Sensing of Environment*, 54, 38–48.
- Facey, V. L., La Duke, J. C., & Wyckoff, A. M. (1986). Vascular plants of Oakville Prairie, North Dakota. *Prairie Naturalist*, 18, 203–210.
- Fensholt, R., & Sandholt, I. (2003). Derivation of a shortwave infrared stress index from MODIS near- and shortwave infrared data in a semiarid environment. *Remote Sensing of Environment*, 87, 111–121.
- Ferreira, L. G., Asner, G. P., Knapp, D. E., Davidson, E. A., Coe, M., Bustamante, M. M. C., et al. (2011). Equivalent water thickness in savanna ecosystems: MODIS estimates based on ground and EO-1 Hyperion data. *International Journal of Remote Sensing*, 32, 7423–7440.
- Filet, P. G. (1994). State and transition models for rangelands. 3. The impact of the state and transition model on grazing lands research, management and extension: a review. *Tropical Grasslands*, 28, 214–222.
- Gao, B. (1996). NDWI—A normalized difference water index for remote sensing of vegetation liquid water from space. *Remote Sensing of Environment*, 58, 257–266.
- Gitelson, A. A., Merzlyak, M. N., & Chivkunova, O. B. (2001). Optical properties and nondestructive estimation of anthocyanin content in plant leaves. *Photochemistry and Photobiology*, 71, 38–45.
- Gitelson, A. A., Zur, Y., Chivkunova, O. B., & Merzlyak, M. N. (2002). Assessing carotenoid content in plant leaves with reflectance spectroscopy. *Photochemistry and Photobiology*, 75, 272–281.
- Government of Alberta (2010). *Grassland vegetation inventory (GVI) specifications*. Alberta Sustainable resource Development. : Government of Alberta (101 pp.).
- Guerszman, J.-P., Hill, M. J., Barrett, D. J., Renzullo, L., Marks, A., & Botha, E. (2009). Estimating fractional cover of photosynthetic vegetation, non-photosynthetic vegetation and soil in mixed tree-grass vegetation using the EO-1 and MODIS sensors. *Remote Sensing of Environment*, 113, 928–945.
- Hansen, M. C., & Loveland, T. R. (2012). A review of large area monitoring of land cover change using Landsat data. *Remote Sensing of Environment*, 122, 66–74.
- Hardisky, M. A., Klemas, V., & Smart, R. M. (1983). The influences of soil salinity, growth form, and leaf moisture on the spectral reflectance of *Spartina alterniflora* canopies. *Photogrammetric Engineering and Remote Sensing*, 49, 77–83.
- Herrick, J. E., Bestelmeyer, B. T., Archer, S., Tigel, A. J., & Brown, J. R. (2006). An integrated framework for science-based arid land management. *Journal of Arid Environments*, 65, 319–335.

- Herrick, J. E., Lessard, V. C., Spaeth, K. E., Shaver, P. L., Dayton, R. S., Pyke, D. A., et al. (2010). National ecosystem assessments supported by scientific and local knowledge. *Frontiers in Ecology and the Environment*, 8, 403–408.
- Hilker, T., Wulder, M. A., Coops, N. C., Seitz, N., White, J. C., Gao, F., et al. (2009). Generation of dense time series synthetic Landsat data through data blending with MODIS using a spatial and temporal adaptive reflectance fusion model. *Remote Sensing of Environment*, 113, 1988–1999.
- Hill, M. J., & Hanan, N. P. (2011). Current approaches to measurement, remote sensing and modelling in savannas: A synthesis. In M. J. Hill, & N. P. Hanan (Eds.), *Ecosystem function in savannas: Measurement and modeling at landscape to global scales* (pp. 515–545). Boca Raton, Florida: CRC Press.
- Hill, M. J., Renzullo, L., Guerschman, J.-P., Marks, A., & Barrett, D. J. (2013). Use of vegetation index VI indicators from Hyperion data to characterize vegetation states within land cover/land use types in an Australian tropical savanna. *IEEE Journal of Selected Topics in Applied Earth Observations and Remote Sensing (JSTARS)*, 6, 309–319 (EO-1 Special Issue).
- Hill, M. J., Roman, M. O., & Schaaf, C. B. (2012). Dynamics of vegetation indices in tropical and subtropical savannas defined by ecoregions and MODIS land cover. *GeoCarto International*, 27, 153–191.
- Hill, M. J., Roxburgh, S. H., Carter, J. O., & McKeon, G. M. (2005). Carbon changes in response to grazing, drought and fire in savanna woodlands of Australia: A scenario approach using 100 years of simulated annual fire and grassland dynamics. *Australian Journal of Botany*, 53, 715–739.
- Hill, M. J., Vickery, P. J., Furnival, E. P., & Donald, G. E. (1999). Using of NOAA AVHRR NDVI and classified Landsat TM data to describe pastures in the temperate high rainfall zone, HRZ of Eastern Australia. *Remote Sensing of Environment*, 67, 32–50.
- Irons, J. R., Dwyer, J. L., & Barsi, J. A. (2012). The next Landsat satellite: The Landsat Data Continuity Mission. *Remote Sensing of Environment*, 122, 11–21.
- Jeltsch, F., Tietjen, B., Blaum, N., & Rossmanith, E. (2011). Population and ecosystem modeling of land use and climate change impacts on arid and semi-arid savanna dynamics. In M. J. Hill, & N. P. Hanan (Eds.), *Ecosystem function in savannas: Measurement and modeling at landscape to global scales* (pp. 257–272). Boca Raton, Florida: CRC Press.
- Jupp, D. L., Datt, B., Lovell, J., Campbell, S., & King, E. A. (2002). *Discussions around Hyperion data: Background notes for the Hyperion Data Users Workshop*. Canberra: CSIRO.
- Kuchler, A.W., 1975. Potential natural vegetation of the conterminous United States (map). American Geographical Society, New York. 1:7,500,000.
- Leach, M. K., & Givnish, T. J. (1999). Gradients in the composition, structure and diversity of remnant oak savannas in southern Wisconsin. *Ecological Monographs*, 69, 353–374.
- Ludeke, K., German, D., & Scott, J. (2009). *Texas Vegetation Classification Project: Interpretative booklet for phase II*. : Texas Parks and Wildlife Department and Texas Natural Resources Information System.
- Ludwig, J. A., Bastin, G. N., Eager, R. W., Karfs, R., Ketner, P., & Pearce, G. (2000). Monitoring Australian rangeland sites using landscape function indicators and ground- and remote-based techniques. *Environmental Monitoring and Assessment*, 64, 167–178.
- Marssett, R. C., Qi, J. G., Heilman, P., Biedenbender, S. H., Watson, M. C., Amer, S., et al. (2006). Remote sensing for grassland management in the arid Southwest. *Range Ecology and Management*, 59, 530–540.
- McPherson, G. R. (1997). *Ecology and management of North American Savannas*. Tucson, AZ: University of Arizona Press (208 pp.).
- Merzlyak, J. R., Gitelson, A. A., Chivkunova, O. B., & Rakitin, V. Y. (1999). Non-destructive optical detection of pigment changes during leaf senescence and fruit ripening. *Physiologia Plantarum*, 106, 135–141.
- Middleton, E. M., Ungar, S. G., Mandl, D., Ong, L., Frye, S., Campbell, P. E., et al. (2013). The Earth Observing One (EO-1) Satellite Mission: Over a decade in space. *IEEE Journal of Selected Topics in Applied Earth Observations and Remote Sensing (JSTARS)*, 1–10 (EO-1 Special Issue, TBD).
- Nagler, P. L., Inoue, Y., Glenn, E. P., Russ, A. L., & Daughtry, C. S. T. (2003). Cellulose absorption index (CAI) to quantify mixed soil-plant litter scenes. *Remote Sensing of Environment*, 87, 310–325.
- NRCS (2011). Ecological Site Information System Database: ESD user guide. USDA-NRCS. <http://esis.sc.egov.usda.gov/Welcom/pgESDWelcome.aspx>
- NRCS (2012a). Ecological site descriptions, Texas, 089a, 221–239, and 578. USDA-NRCS. <http://esis.sc.egov.usda.gov/Welcom/pgReportLocation.aspx?type=ESD>
- NRCS (2012b). Ecological site descriptions, North Dakota, 055b, 056–077, 056\_087–194. USDA-NRCS. <http://esis.sc.egov.usda.gov/Welcom/pgReportLocation.aspx?type=ESD>
- NRCS (2012c). Ecological site descriptions, Montana, 046x, 250–264, 589–601. USDA-NRCS. <http://esis.sc.egov.usda.gov/Welcom/pgReportLocation.aspx?type=ESD>
- Pearlman, J. S., Barry, P. S., Segal, C. C., Shepson, J., Beiso, D., & Carman, S. L. (2003). Hyperion, a space-based imaging spectrometer. *IEEE Transactions on Geoscience and Remote Sensing*, 41, 1160–1173.
- Pickup, G., & Chewings, V. H. (1994). A grazing gradient approach to land degradation assessment in arid areas from remotely-sensed data. *International Journal of Remote Sensing*, 15, 597–617.
- Potapov, P. V., Turubanova, S. A., Hansen, M. C., Adusei, B., Broich, M., Altstatt, A., et al. (2012). Quantifying forest cover loss in Democratic Republic of the Congo, 2000–2010, with Landsat ETM + data. *Remote Sensing of Environment*, 122, 106–116.
- Schmidt, M., Udelhoven, T., Gill, T., & Röder, A. (2012). Long term data fusion for a dense time series analysis with MODIS and Landsat imagery in an Australian savanna. *Journal of Applied Remote Sensing*, 6, 063512, <http://dx.doi.org/10.1117/1.JRS.6.063512>.
- Sims, D. A., & Gamon, J. A. (2002). Relationships between leaf pigment content and spectral reflectance across a wide range of species, leaf structures and developmental stages. *Remote Sensing of Environment*, 81, 337–354.
- Somers, B., & Asner, G. P. (2012). Hyperspectral time series analysis of native and invasive species in Hawaiian rainforests. *Remote Sensing*, 4, 2510–2529.
- Somers, B., & Asner, G. P. (2013). Multi-temporal hyperspectral mixture analysis and feature selection for invasive species mapping in rainforests. *Remote Sensing of Environment*, 136, 14–27.
- Summers, D., Lewis, M., Ostendorf, B., & Chittleborough, D. (2011). Visible near infrared reflectance spectroscopy as a predictor of soil properties. *Ecological Indicators*, 11, 123–131.
- Svingen, D., Braun, B., & Gonzalez, M. (2008). *Sheyenne National Grassland's Ecological Assessment and Restoration Strategy: 2008*. Dakota Prairie Grasslands, internal report.
- Tucker, C. J. (1979). Red and photographic infrared linear combinations for monitoring vegetation. *Remote Sensing of Environment*, 8, 127–150.
- Tucker, C. J., Justice, C. O., & Prince, S. D. (1986). Monitoring the grasslands of the Sahel 1984–1985. *International Journal of Remote Sensing*, 7, 1571–1581.
- Tueller, P. T. (1989). Remote sensing technology for rangeland management applications. *Journal of Range Management*, 42, 442–453.
- Ustin, S. L., Gitelson, A. A., Jacquemoud, S., Schaepman, M., Asner, G. P., Gamon, J. A., et al. (2009). Retrieval of foliar information about plant pigment systems from high resolution spectroscopy. *Remote Sensing of Environment*, 113, S67–S77.
- Ustin, S. L., Roberts, D. A., Gamon, J. A., Asner, G. P., & Green, R. O. (2004). Using imaging spectroscopy to study ecosystem processes and properties. *Bioscience*, 54, 523–534.
- Weber, G. E., Moloney, K., & Jeltsch, F. (2000). Simulated long-term vegetation response to alternative stocking strategies in savanna rangelands. *Plant Ecology*, 150, 77–96.
- Westoby, M., Walker, B. H., & Noy-Meir, I. (1989). Opportunistic management for rangelands not at equilibrium. *Journal of Range Management*, 42, 266–274.
- Wulder, M. A., Masek, J. G., Cohen, W. B., Loveland, T. R., & Woodcock, C. E. (2012). Opening the archive: How free data has enabled the science and monitoring promise of Landsat. *Remote Sensing of Environment*, 122, 2–10.
- Yang, L., Wylie, B. K., Tieszen, L. L., & Reed, B. C. (1998). An analysis of relationships among climate forcing and time-integrated NDVI of grasslands over the US Northern and Central Great Plains. *Remote Sensing of Environment*, 65, 25–37.
- Yilmaz, M. T., Hunt, E. R., & Jackson, T. R. (2008). Remote sensing of vegetation water content from equivalent water thickness using satellite imagery. *Remote Sensing of Environment*, 112, 2514–2522.